Titre: Title:	Force Analysis of Minimal Self-adaptive Fingers Using Variations of Four-Bar Linkages
Auteur: Author:	Fadi Nassar
Date:	2021
Type:	Mémoire ou thèse / Dissertation or Thesis
Référence: Citation:	Nassar, F. (2021). Force Analysis of Minimal Self-adaptive Fingers Using Variations of Four-Bar Linkages [Mémoire de maîtrise, Polytechnique Montréal]. PolyPublie. https://publications.polymtl.ca/9182/

URL de PolyPublie: PolyPublie URL:	https://publications.polymtl.ca/9182/
Directeurs de recherche: Advisors:	Lionel Birglen
Programme: Program:	Génie mécanique

POLYTECHNIQUE MONTRÉAL

affiliée à l'Université de Montréal

Force Analysis of Minimal Self-adaptive Fingers Using Variations of Four-Bar Linkages

FADI NASSAR

Département de génie mécanique

Mémoire présenté en vue de l'obtention du diplôme de *Maîtrise ès sciences appliquées*

Génie mécanique

Aout 2021

POLYTECHNIQUE MONTRÉAL

affiliée à l'Université de Montréal

Ce mémoire intitulé :

Force Analysis of Minimal Self-adaptive Fingers Using Variations of Four-Bar Linkages

présenté par **Fadi NASSAR**

en vue de l'obtention du diplôme de *Maîtrise ès sciences appliquées*

a été dûment accepté par le jury d'examen constitué de :

Farbod KHAMENEIFAR, président

Lionel BIRGLEN, membre et directeur de recherche

Bruno BELZILE, membre

ACKNOWLEDGEMENT

First, I would like to thank my director of research, Lionel Birglen, for all his support and help throughout this research. Thank you for proposing this subject and trusting me. I would like also to thank my parents, Ghada and Zouheir, and siblings, Noha and Samer, who were supporting me in every mean they could on every step of the way, thousands of miles away and in the most difficult of times.

To the members of the robotics laboratory, Nicolas et Ian, I say thank you for the time spent together, whether working or having fun.

I would finally like to thank all my family and friends; I am truly grateful for the presence of such wonderful people in my life.

RESUME

Les préhenseurs sont l'un des éléments les plus critiques et les plus importants dans le domaine de la robotique car elles sont le moyen par lequel le robot interagit avec son environnement. L'utilisation typique d'un actionneur pour chaque degré de liberté (DDL) de la pince conduit généralement à des conceptions très complexes et à des algorithmes avancés pour le contrôle des moteurs et des capteurs impliqués. Cependant, les pinces auto-adaptatives ou aussi communément appelées sous-actionnées ont généralement une conception et un contrôle beaucoup plus simples du fait de leur capacité à s'adapter à la forme de l'objet à saisir. Par conséquent, les pinces auto-adaptatives font l'objet d'un nombre croissant de recherches en raison de leur faible coût et de leur simple fabrication et contrôle.

Par rapport aux recherches précédentes, ce travail ne vise pas à rendre les doigts auto-adaptatifs plus capables mais plus simples. Une tendance courante dans la recherche est de se concentrer sur l'amélioration des solutions existantes en ajoutant de nouvelles pièces, capteurs ou actionneurs, ce qui complexifie souvent les conceptions. Une autre approche, tout comme l'approche proposée ici, consiste à rendre la conception aussi simple que possible et à analyser le compromis qui en résulte entre complexité et performance. Dans ce but, quatre versions de doigts auto-adaptatifs basés sur le mécanisme à un DDL le plus simple, le mécanisme à quatre barres, sont présentées dans ce travail. Cependant, quatre variantes de ce mécanisme sont discutées, dont certaines avec un joint prismatique. Ces doigts sont conçus dans le but d'être attachés et utilisés avec les mêmes pinces de translation standard que l'on trouve dans les industries de fabrication et d'emballage car elles sont aussi simples à contrôler que les mâchoires monolithiques standard, mais offrent également une adaptabilité de forme aux objets.

Le but ultime de ce travail est d'évaluer si les liaisons les plus simples pour les doigts adaptatifs peuvent produire le même niveau de performance en termes de forces de préhension que des conceptions plus complexes. À cette fin, des recherches antérieures sont d'abord présentées afin d'acquérir plus de connaissances sur le sujet. Une analyse de force et une optimisation sur les quatre conceptions à l'aide d'une analyse kinétostatique et de trois critères d'optimisation sont ensuite présentées et les résultats sont présentés et discutés. Enfin, trois conceptions potentiellement plus efficaces avec des joints prismatiques sont présentées.

À la lumière de cette étude, il est montré que des conceptions plus simples ne signifient pas nécessairement des performances plus faibles, car les résultats peuvent être considérés comme au moins comparables à d'autres conceptions entièrement actionnées.

ABSTRACT

Grippers are one of the most critical and important elements in the field of robotics because they are the means by which the robot interacts with its surroundings. The typical use of one actuator for each degree-of-freedom (DOF) of the gripper generally leads to very complex designs and advanced algorithms for the control of the motors and the sensors involved. However, self-adaptive or also commonly called underactuated grippers generally have a much simpler design and control because of their ability to adapt to the shape of the object to be seized. Therefore, self-adaptive grippers are the focus of a growing number of research because of their low cost and simple manufacturing and control.

Compared to previous research, this work does not aim at making self-adaptive fingers more capable but simpler. One common trend in research is to focus on improving existing solutions by adding new parts, sensors, or actuators, often complexifying designs. Another, just like the approach proposed here, is to focus on making the design as simple as possible and to analyse the resulting trade-off between complexity and performance. To this aim, four versions of self-adaptive fingers based on the simplest one DOF linkage, the four-bar linkage, are presented in this work. However, four variations of four-bar linkages are discussed including some with a prismatic joint. These fingers are designed with the aim of being attached to and used with the same standard translational grippers as one finds in the manufacturing and packaging industries since they are as simple to control as the standard monolithic jaws, but also offer shape adaptability to the objects.

The ultimate purpose of this work is to evaluate whether simplest linkages for adaptive fingers can produce the same level of performance in terms of grasp forces as more complex designs. To this aim, previous research is presented first in order to gain more knowledge on the topic. A force analysis and optimization on the four designs using a kinetostatic analysis and three optimization criteria are then presented and results are shown and discussed. Finally, three potentially more efficient designs with prismatic joints are presented.

In the light of this study, it is shown that simpler designs do not necessarily mean weaker performance, as the results can be considered at least comparable with other fully actuated designs.

TABLE OF CONTENTS

LIST OF TABLES

LIST OF FIGURES

LIST OF APPENDICES

CHAPTER 1 INTRODUCTION

The research work presented in this thesis is under the supervision of Professor Lionel Birglen and is a continuation of his work on underactuated robotic fingers carried out at the Robotics Laboratory of École Polytechnique de Montréal. The objective is to evaluate the performances of simpler geometries of designs of self-adaptive fingers based on variations of four-bar mechanisms using prismatic joints.

A gripper is the element that makes it possible for a robotic system to come into direct contact with the environment around it in order to grasp or manipulate or in general interact with objects. The gripper is as critical to robots as the hand is to humans. Moreover, the human hand remains unrivaled in terms of versatility, dexterity and skill, and it is why many have sought to mimic its operation and emulate its functionalities. However, according to (Tubiana, Thomine, & Mackin, 1998), the human hand has 17 joints, 19 bones and uses 19 muscles, which makes it a very complex mechanism. Instead of using a large number of actuators (muscles in the case of the human hand) whose operation is coordinated by a complex control system (the nerves and the brain in the case of the human hand), adaptive grippers have the ability to adapt to their environment. Thus, by designing an intelligent mechanical system capable of adapting passively to an object, it is no longer necessary to use as many sensors and actuators as there are degrees of freedom (DOF).

1.1 Underactuated self-adaptive robotic fingers

Artificial grippers are used in various fields where the use of the human hand is impractical or even impossible. Many sectors are the subject of studies on artificial grippers. The industrial and prosthetic applications are the most widely known fields, but other ones also contribute to this line of research, in particular that of robotic surgery (Kota, et al., 2005); (Doria & Birglen, 2009) and that of the space domain (Nakanishi & Yoshida, 2002). A gripper can perform many functions that can be divided into three broad categories, namely the grasping of objects, their manipulation and the ability to make gestures. For the function of grasping objects, (Cutkosky, 1989) presents a relatively complete classification of the types of holds achievable by one hand. However, by limiting the scope to the planar case, one can identify two main ones, namely the enveloping grip and the pinch grip. In the case of the enveloping grip, it is desired to maximize

the number of contacts points. This has the advantage of obtaining a more rigid grip and a more uniform distribution of contact forces. Thus, the risk of damaging fragile objects is reduced (Kragten & Herder, 2010); (Krut, 2005). As for the pinch grip, also called precision grip, it allows the grip of smaller objects or objects with flat sides with more precision (Birglen & Herbecq, 2009); (Begoc, Krut, Dombre, Durand, & Pierrot, 2007); (Gosselin & Laliberte, 1998). Manipulating an object is the act of changing its position and/or orientation. In an industrial context, the gripper is generally attached to a manipulator robot which will accomplish this task. However, the ability to manipulate an object within the socket can be useful in the case of a prosthesis or for other specific applications. For example, the Robonaut Hand by (Diftler, Ambrose, Tyree, Goza, & Huber, 2004) is able to reorient an object when it is grasped with the fingertips by moving them one after the other. The ability to gesture is generally only sought in the design of robotic prostheses. It can be defined as the ability to perform distinct free movements. For example, the SmartHand of (Cipriani, Controzzi, & Carrozza, 2010) is a robotic hand intended for use in prosthetics and is capable of performing simple gestures such as pointing or counting on fingers while other concepts simply seek to mimic the behavior of human fingers (Figliolini & Ceccarelli, 2002); (Ceccarelli, Rodriguez, & Carbone, 2006).

The principle of underactuation is defined by the use of a lower number of actuators compared to the number of DOFs and can be applied on artificial grippers. At the scale of a robotic hand, underactuation is achieved when several fingers are driven by the same actuator, and at the scale of a single finger, it is when one actuator drives multiple phalanges as long as there are more DOFs in the finger. The configuration of the underactuated fingers is not fully defined by the position of the actuator (s). If properly designed, these fingers have the ability to passively adapt to the object grasped. This is why they are also called adaptive fingers. To constrain the placement of the finger when it is not in contact with an object, passive elements such as springs and stops are generally used (Gosselin & Laliberte, 1998). However, some concepts are based on the use of a return tendon, for example the Soft Gripper (Hirose & Umetani, 1978), or on the intrinsic rigidity of the compliant mechanisms (Doria & Birglen, 2009); (Boudreault & Gosselin, 2006); (Lotti & Vassura, 2002). A typical example of the operation taken from (Birglen & Gosselin., 2006) of such a mechanism applied to a finger is shown in 1.1 Closure of a 2-DOF finger on an object, taken from . We can observe that there is no relative movement between the

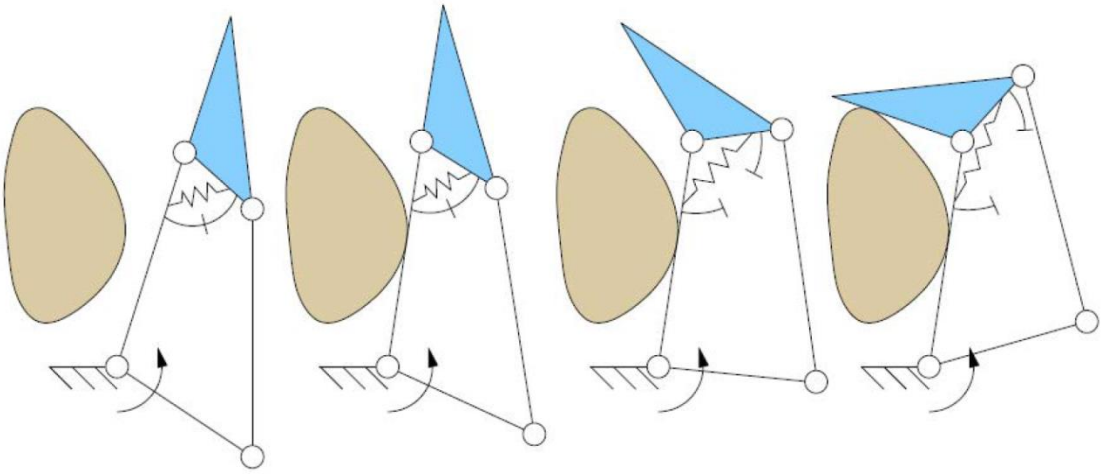

1.1 Closure of a 2-DOF finger on an object, taken from (Birglen & Gosselin., 2006)

two phalanges before the first contact with the object, these being in abutment. Once the proximal phalanx is in contact with the object, the actuating torque increases so much so that the torque applied to the distal phalanx exceeds that of the spring which held it in abutment. The latter therefore closes on the object until there is contact. If the finger is in static equilibrium, then the grip is complete.

1.2 Problematic

The manufacturing and packaging industry still mostly relies on linear actuators for mechanical grippers for their operations, as discussed in more details in section 2.3. These industries are reluctant to change the grippers since they have been using them for decades now. Even if adaptive hands have an advantage in terms of simplicity of control over fully actuated designs, and in shape adaptiveness over monolithic jaws, the cost of adjusting the adaptive grippers to the robots or machines is still high. A solution for this problem is presented in (Birglen, 2015), where a 3-DOF self-adaptive finger that could be actuated by a translating movement in its base is introduced. A similar idea already existed and is embodied in the FinGripper, designed by EvoLogics GmbH, now commercialized by Festo. However, a simplified design with only two revolute joints in the transmission linkage (2-DOF) was studied in (Birglen, 2019), and it was evidenced by experimental results that having phalanges with full mobility is arguably not critical to ensure a successful grasp. It should be noted that even though the 2-DOF finger presented in (Birglen, 2019) is also actuated by a linear motion of the base, it was specifically designed for the

use with collaborative robots and not for industrial robots/machines. Further increasing the simplicity of self-adaptive fingers was studied in various works. (Kok & Low, 2018) presents a 1-DOF self-adaptive finger using a translational actuator at the base and its enveloping and pinch grasps were analysed, but the work was more focused on the shape adaptability of the fingers and the contact points with the objects to be seized than the forces generated by the finger. Another example of 1-DOF fingers is presented in (Abdeetedal & Mehrdad, 2018) with force analysis, but the actuation is a rotational one.

When talking about what mechanical joints to use in the design of self-adaptive fingers, rotational joints is the first, if not only one that comes to mind. The use of prismatic joints is not common in the design of self-adaptive fingers and the work related to it is very rare in the literature. This type of mechanical joints is generally harder to manufacture than rotational ones and its design and integration in self-adaptive fingers is more demanding (placement of the translational axis, direction of the linear movement, etc.).

1.3 Research objectives

In order to develop new simple designs of self-adaptive fingers for industrial applications while still being performant and to quantify the effect of using prismatic joints in the mechanisms of these fingers, the objective of this research is to evaluate the performances of simple 1-DOF self-adaptive fingers based on variations of the four-bar linkage with a linear actuation at the base.

The specific objectives are identified as:

1. Develop a kinetostatic model of four underactuated fingers with varying numbers of phalanges and kinematic pairs used in the mechanism:
    a) Two phalanges, all revolute joints.
    b) Two phalanges, one prismatic joint.
    c) Three phalanges, all revolute joints.
    d) Three phalanges, one prismatic joint.
2. Choose or define performance criteria.
3. Optimize the chosen architectures, for each of the selected combinations, against the performance criteria determined previously.
4. Compare the performance of the different optimized concepts.

CHAPTER 2 LITERATURE REVIEW

2.1 Four-bar mechanisms

A four-bar linkage, also commonly known as a four-bar, consists of four members connected in a loop by four joints. The most common four-bars are configured so the links move in one plane or in parallel planes, in this case it is called a planar four-bar. Spatial and spherical four-bars are also used sometimes in practice as mentioned in (Hartenberg & Denavit, 1964).

2.1.1 Planar four-bar

In a planar four-bar mechanism, a joint can be either a revolute (R) or a prismatic (P), since they are the only planar lower pairs. As for the members, or links, one can differentiate between a crank which is a link connected to the ground by a revolute joint, and a slider which is a link connected to the ground by a prismatic joint. A crank can also be called a rocker when it physically can't complete a full rotation about the center of the revolute joint. The third moving member of the four-bar is called a floating link or coupler if it connects two cranks or connecting rod if it connects a crank to a slider.

Depending on the combination of prismatic and revolute joints used, one can find three basic types of planar four-bar mechanisms: The planar quadrilateral, the crank-slider, and the double-slider.

2.1.1.1 Planar quadrilateral

Denoted RRRR or 4R, this four-bar is formed by four members: two cranks, a coupler, and a fixed link; and four revolute joints. As demonstrated in (Norton, 2003), this type of mechanisms can have three different types of motion depending on the dimensions of its members. In the first type of motion of this mechanism, both of the members connected to the fixed one can rotate a full rotation about their respective joint axis. This type of four-bar is commonly known as a "double-crank". In the second type, only one of the two members connected to the fixed link can make a full rotation and the other one can only oscillate. This four-bar is called "crank-rocker". The third type is called "double-rocker", and in this one both of the links connected to the fixed

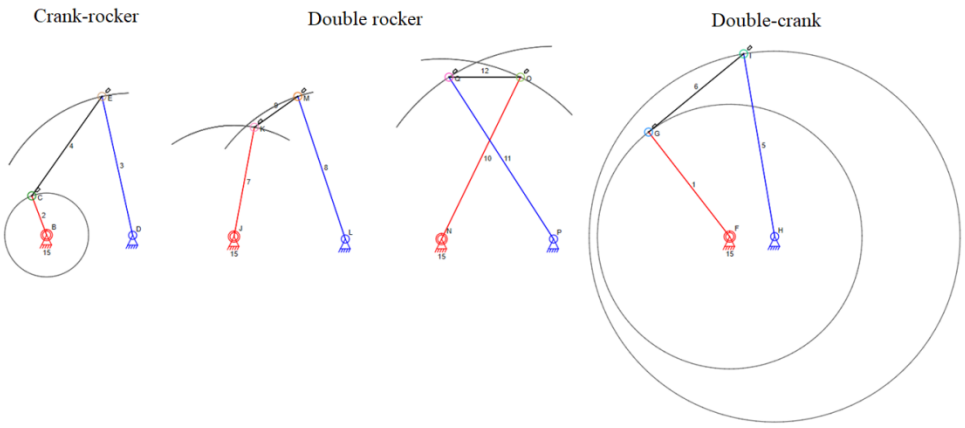

Figure 2.1 Types of motion of the quadrilateral four-bar

one can only oscillate about their joint axis. Grashof's theorem states that if the sum of the shortest and longest members is less than or equal to the sum of the two remaining members, then the shortest member can make a full rotation. This condition is then satisfied if:

$$S + L \leq P + Q \tag{2.1}$$

Where S is the length of the shortest member, L is the length of the longest member, and P and Q are the lengths of the two remaining members. Another way to classify the motion of this four-bar is to consider the three terms T_1, T_2, and T_3 :

$$\begin{aligned} T_1 &= f + c - i - o \\ T_2 &= o + f - i - c \\ T_3 &= o + c - i - f \end{aligned} \tag{2.2}$$

where i is the length of the input link, o the length of the output link, and f and c are the lengths of the fixed member and the coupler respectively. Depending on the combination of those three terms, one can classify the mobility of the four-bar like shown in the Table 2.1. In the first four rows of the table and the last one, the Grashof condition is satisfied so one link in the mechanism can make a full rotation, and it could be one of the three links: right side link, left side link, or the

coupler. In the fifth row, the Grashof condition is not satisfied, so no link in the mechanism can make a full rotation. For all of the combinations of T_i the mechanism is a double rocker no matter what the shortest link is. There is one special case where $T_i = 0 \; \forall \; i$, and in this case the mechanism folds on itself for a certain input angle This type is commonly called "Change point".

Table 2.1 Classification of the quadrilateral four-bar function of the link dimensions

Case	T_1	T_2	T_3	**Grashof cond.**	**Input link**	**Output link**	**l+s vs p+q**	**Shortest bar**	**Type**
1	-	-	+	Grashof	Crank	Crank	<	Frame	Double-crank
2	+	+	+		Crank	Rocker		Side	Crank-rocker
3	+	-	-		Rocker	Crank		Side	Rocker-crank
4	-	+	-		Rocker	Rocker		Coupler	Double rocker
5	-	-	-	Non-Grashof	Rocker	Rocker	>	Any	Double rocker
	-	+	+		Rocker	Rocker			Double rocker
	+	-	+		Rocker	Rocker			Double rocker
	+	+	-		Rocker	Rocker			Double rocker
6	0	0	0	Grashof	Crank	Crank	=	Any	Change point

When designing an RRRR linkage, one should take into consideration different aspects of the mechanism when aiming to produce a certain output motion for a specific input. The lengths of the members of a mechanism have to be determined by dimensional synthesis which is a process based on iterating and analyzing the results, however, in some scenarios, exact and detailed methods to give accurate dimensions for the links of the mechanism may not work. (Toussaint, 2003) presents some of the aspects to consider when designing an RRRR four-bar:

2.1.1.2 Time ratio

In a crank-rocker type of four-bars, the input member can make a full rotation about the rotational joint connecting it to the fixed member while the output member can only go back and forth on a

certain circular path. The time ratio Q of the mechanism defines numerically how fast the first stroke is compared to the second, faster stroke:

$$Q = \frac{Time\ of\ slower\ stroke}{Time\ of\ quicker\ stroke} \geq 1 \tag{2.3}$$

The total cycle time Δt_{cycle} for the mechanism is the sum of the time taken to finish the first stroke and the time taken to finish the second one. It can be used to find the rotational speed of the crank since it can rotate full rotations:

$$\omega_{crank} = (\Delta t_{cycle})^{-1} \tag{2.4}$$

2.1.1.3 Transmission angle

It is important to understand how the mechanism will operate when exerting external forces while the kinematic characteristics of the mechanism are considered. Mechanism performance is the effective transmission of motion and forces from the input to the output member. In other words, for a constant torque applied on the input member, one has to get the maximum possible output torque from the rocker and minimum bearing forces in a high performance mechanism. The transmission angle is given by:

$$\sin \mu = \frac{Force\ component\ that\ tends\ to\ move\ the\ output\ member}{Total\ force\ applied\ to\ the\ output\ member} \tag{2.5}$$

2.1.1.4 Dead point

In a crank-rocker mechanism, the rocker is oscillating in a certain circular arc when the crank is making full and continuous rotations, and this means that the velocity of the rocker is null when it attains its limit positions. These positions are called dead points and they are attained when the crank becomes aligned with the coupler. When this happens, the crank can only be compressed or extended, and a torque applied to the rocker cannot induce rotation in the crank.

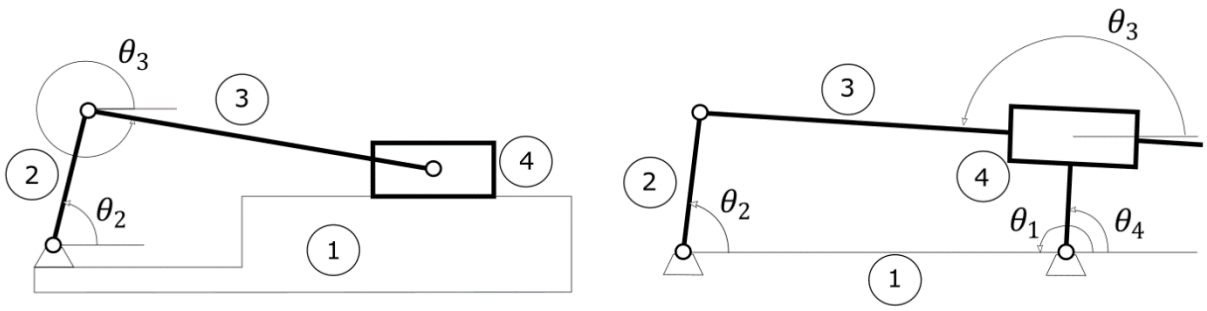

Figure 2.2 Input/Output parameters of the two versions of the slider-crank

2.1.2 Slider-crank

In the slider-crank mechanism, a rotational joint is replaced by a prismatic one to obtain finally three rotational joints and one prismatic. Its most known application is in engines, where the expanding gas in the cylinder will cause the piston to slide and then drive the rotation of the crank. As seen in Figure 2.2, one can differentiate between two types of crank-slider mechanisms:

On the left side of the figure, the standard version of the crank-slider is shown. Link #1 is the ground, which is the base and reference link. Link #2 is most commonly the input link, which is controlled by the input angle θ_2 and link #4 is the slider, generally considered as the output link. The horizontal distance between the slider and a fixed point in the ground is the output variable of this mechanism. Link #3 is the coupler with angular position θ_3 and it connects the input link to the output slider. For this version, one can find two different sub-types depending on the axis of the prismatic joint. The in-line slider-crank, where the slider of the mechanism is positioned so that the line of travel of the hinged joint of the slider intersects with the axis of the revolute joint connecting the base of the mechanism with the crank, and the offset slider-crank, where the axis of the prismatic joint does not intersect the axis of the rotational joint of the base and the crank, creating a forward movement slower than the return movement. It is also called a quick-return mechanism.

On the right side is an illustration of the inverted slider-crank mechanism. Link #1 is the ground link, link #2 is the input link which is controlled by the angle θ_2 and the link number 4 is the

slider (output link). The main difference between the two mechanisms, as discussed in (Myszka, 2012), is that for the inverted crank-slider, the slider is connected to the ground via a revolute joint and to the coupler via a prismatic joint, while the first one has the opposite configuration. Therefore, the output variable can be the angle θ_4 of the slider with the length AB being the input.

2.1.3 Double-Slider

Four-bar linkages with two prismatic joints also exist and they are called double-sliders. Its most common design is made up of two sliders, a frame in which the slider moves, and a link that connects the two sliders and fixes the distance between them. This specific geometry was used in (Guangbo & Zhu, 2019) to design a monolithic compliant gripper. Other geometries also exist for this linkage where the rotational joint is not on top of the slider, like the Assure IV/3 linkage studied in (Almestiri, Murray, Myszka, & Wampler, 2016). This linkage was not used for the design of a self-adaptive gripper here because in (Guangbo & Zhu, 2019) the actuation of the mechanism is a vertical translating motion of the base, which is not the case in the context of this thesis, and the study in (Almestiri, Murray, Myszka, & Wampler, 2016) showed that this mechanism has limited ranges for its link dimensions for it to generate motion.

2.2 Spatial four-bar

The structure of spatial four-bar linkages is more complex when compared with planar four-bar linkages. As a result, studies on the path synthesis and analysis of spatial four-bar linkages are relatively few. The most common spatial four-bar is the spherical four-bar linkage. It is widely used in grippers (Kocabas, 2009), wings (McDonald & Agrawal, 2010), wrists (Hess-Coelho, 2007), and surgical robots (Wu, Liu, Wang, & Wang, 2010) . The spherical four-bar linkage has four members and four rotational joints having their axes intersecting in a single point and they move in concentric spheres. Another example of a spatial four-bar is the Bennett linkage, which has been recognized as a building block for the construction of more complex mechanisms, like the 6R mechanisms presented in (Song, Chen, & Chen, 2013). It comprises four links functioning as common perpendiculars between adjacent pairs of the four revolute joints that connect them.

The linkage is most commonly used in the aerospace domain (Yu, Luo, & Li, 2007), and in the design of antennae (Song, et al., 2017).

2.3 Industrial grippers

Grippers are used in the industry to handle objects. These objects are generally workparts that are to be moved by a robot. The applications of the part handling operations include machine loading and unloading, picking parts from a conveyor, and arranging parts onto a pallet. In addition to workparts, other objects could be handled by robotic grippers like cartons, bottles, raw materials, and tools. (Reddy & Suresh, 2013) presents in detail the different types of grippers used in the industry, and they can be divided into five main types.

The first type is the vacuum gripper, which has been a standard tool for robots in manufacturing applications because of its high level of flexibility. It is made of polyurethane or rubber suction cups to grasp and handle objects. The second type is the magnetic gripper and they're exclusively used for holding ferrous workparts since they are based on the principles of magnetism. Some grippers use permanent magnets in addition to a device called stripper push to separate the object, while others, called electromagnetic grippers use a controller unit and a DC power source. The three remaining types are the hydraulic, pneumatic, and servo-electric grippers. They all require mechanical linkages to function and the difference between them is the type of actuation. In hydraulic grippers the force is provided from pumps that can generate up to 13700 kPa (Escriva, 2016) making them the go-to gripper for applications that require a huge amount of force. Pneumatic grippers are popular due to their light weight and compact size, and are most commonly designed for operations in tight spaces which is also helpful in the manufacturing industry (Escriva, 2016). It should be noted that hydraulic and pneumatic grippers are actuated by a linear motion at the base of the gripper. Servo-electric grippers are very flexible and convenient for handling different material tolerances. They are becoming very popular in industry because of their simplicity in control, which is done by electric motors, whether linear or rotational.

For the last three types of grippers, monolithic jaws are most commonly used because of their simplicity in manufacturing and usage. But the shapes of the objects to handle are becoming more and more complex and these jaws are becoming less convenient for the general applications

in the industry. This is why self-adaptive / underactuated fingers are becoming popular in this domain. Many companies commercialized to the public and the industry underactuated hands and fingers in the last decade, such as Robotiq's 2F-85 and 2F-140 Adaptive Grippers.

2.4 Self-adaptive robotic grippers

Self-adaptive robotic fingers are considered a mainstream topic in both the research community and the industry. They have been attracting attention during the last decade because they are simpler, from a mechatronic perspective, than fully actuated designs: They can be controlled with a simple on/off command, they don't need sensors, and they typically require only one actuator. The first prototype presented to the research community is the Soft Gripper of Prof. Hirose (Hirose & Umetani, 1978) and it has ten phalanges controlled by two wires, and it inspired other designs with three phalanges that became much more common (Dollar & Howe, 2006), (Catalano, et al., 2012), (Ozawa, Hashirii, & Kobayashi, 2009).

2.4.1 Analysis

After completing the design of the self-adaptive finger, there is little control over the behavior of that finger because not every one of its degrees of freedom is controlled independently. Thus, the characteristics of the grasp, i.e. the configuration of the finger, the location of the contact points and the forces exerted, depend on the object to be seized and on the geometry of the transmission linkage. For this reason, it is important to design underactuated fingers methodologically. Since the principal task of a gripper is to grasp an object, the main problem lies in assessing the ability of a finger to exert contact forces, see (De Visser & Herder, 2000). For underactuated fingers, this is not as straightforward as it is for the fully actuated ones. The effect of the actuator on the phalanges changes since the configuration of the transmission mechanism also changes with the configuration of the phalanges. In this sense, an analytical method based on a kinetostatic analysis to calculate the contact forces of an underactuated finger for a given contact configuration is proposed in (Birglen & Gosselin, 2003) (i.e. the localization of the contact points on the phalanges and the configuration of the finger). In a kinetostatic analysis, the input motion is pre-defined and the goal is to calculate the forces or torques that are required to perform the pre-defined motion. A new so-called transmission matrix is presented and used, along with a

Jacobian matrix, to calculate the resulting torque at the base of each of the phalanges as a function of torque or actuation force. This model is intended to be general and applicable to any architecture. However, there remains the problem of calculating the final configuration of the finger. The finger has to be in static equilibrium in order to perform a stable grip on an object. Assuming that the object is fixed, and defining a positive contact force corresponding to a phalanx pushing on the object, the finger is in static equilibrium as long as no contact force becomes negative, see (Birglen & Gosselin, 2003). If this happens, then the configuration of the finger will change, starting with the loss of contact at that location. This development was first observed by (Kaneko & Tanie, 1994), whose work included the calculation of the location of the contact point in equilibrium. However, sometimes the grip does not reach a stable configuration and the phalanges slide over the object until it is ejected. This ejection phenomenon, first mentioned in (Laliberté & Gosselin, 1998), is illustrated in Figure 2.4a). Ejection can also occur in hyperextension, see Figure 2.4b).

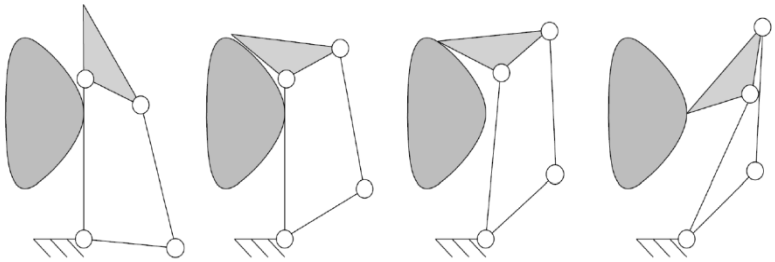

Figure 2.4a) Example of an ejection sequence, taken from (Birglen, Laliberté, & Gosselin, 2007)

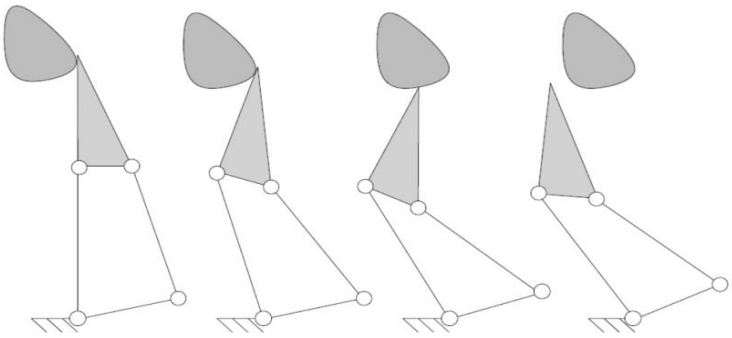

Figure 2.4b) Example of a hyperextension ejection sequence, taken from (Birglen, Laliberté, & Gosselin, 2007)

Several works discuss the reconfiguration of underactuated fingers. Among these, (Birglen & Gosselin, 2003) worked on two DOF fingers and established their reconfiguration and the conditions ensuring their stability. In (Birglen, Laliberté, & Gosselin, 2007), the analysis is taken further for fingers with three phalanges, but no general analytical method has been proposed to determine whether the finger is stable or not although several conditions influencing stability have been identified. A numerical approach is however proposed in (Khakpour & Birglen, 2013).

2.4.2 Optimization

As mentioned earlier, the design phase of the underactuated fingers is important, as there is not much control over the behavior of the finger afterwards. Several criteria are used in the literature to assess the performance of adaptive fingers and thereby help in their design. The article (Kragten & Herder, 2010) provides a good summary on this subject. The criteria fall into two

categories, those that evaluate a finger without considering a specific object to be grasped, and those that consider specific objects.

2.4.2.1 General objects

Among the optimization metrics that do not consider an object, we find the closure trajectory, or preshaping, which is the trajectory that a finger follows before coming into contact with an object. Different closing paths can be looked for when designing a robotic finger. For example, some concepts simply seek to mimic the behavior of human fingers ((Figliolini & Ceccarelli, 2002); (Ceccarelli, Nestor, & Giuseppe, 2006)). In other cases, it is rather the type of grip desired that will dictate the approach course. For example, to achieve a pinch grip, a path in which the distal phalanx remains perpendicular to the palm of the hand is generally preferred. However, we can add to those metrics the workspace, defined as the range of movement covered by the joints. In terms of forces, there are four main criteria. Stability, in the form of a grip stability plan, cf. (Birglen, Laliberté, & Gosselin, 2007), or as an optimization criterion, cf. (Begoc, Krut, Dombre, Durand, & Pierrot, 2007), is often used. There is also the distribution of forces, generally considered for the purpose of obtaining an isotropic distribution of forces ((Hirose & Umetani, 1978); (Krut, 2005)). The magnitude of forces can be of interest, whether to maximize or minimize them. Finally, the direction of the force resulting from all contact forces can give an indication of the capacity of the finger to produce rigid grips. Indeed, the force must be directed towards the palm and towards the opposite finger to resist external forces, cf. (Boudreault & Gosselin, 2006).

2.4.2.2 Specific objects

For criteria taking into account specific objects, (Kragten & Herder, 2010) distinguish three sub-categories, namely criteria based on contact forces, the ability to grasp an object and the ability to hold an object. In the first one, one can find the distribution of contact forces, still looking for isotropy (Hirose & Umetani, 1978); (Gosselin, Pelletier, & Laliberte, 2008). However, in (Kamikawa & Maeno, 2008), the aim is rather to achieve a distribution of forces comparable to that of human fingers. The magnitude of the forces is still used as a criterion in (Gosselin, Pelletier, & Laliberte, 2008), where it is maximized with respect to the actuating torque. In contrast, in (Dollar & Howe, 2006), contact forces are minimized to avoid damage to fragile

objects. Again, obtaining a resultant force pushing the object towards the palm and towards the opposite finger has also been a design objective used with specific objects (Birglen, Laliberté, & Gosselin, 2007); (Laliberté & Gosselin, 1998); (Gosselin, Pelletier, & Laliberte, 2008).

2.4.3 Successful grasps

The ability to grasp an object can take several definitions depending on what is meant by a successful grasp. We can maximize the number of different objects and initial positions in relation to the gripper for which the latter will manage to complete a grip. Sometimes it is the variety of objects and positions (the object being fixed) for which the finger arrives at a stable configuration that is maximized, cf. (Sie & Gosselin, 2002). Prototypes have also been evaluated by testing their ability to grasp objects that are not supported by their environment, for example in (Kamikawa & Maeno, 2008).

Finally, the ability to hold an object was approached in three main ways. In (Bégoc, Durand, Krut, Dombre, & Pierrot, 2006), the way to determine form closure was adapted to underactuated fingers. Then, the ability to resist external forces has been experimentally evaluated, among others by (Kamikawa & Maeno, 2008). Finally, the stiffness of the grip was quantified in (Kragten & Herder, 2010) by the work required to move an object within the grip. The work required to extricate an object from the grip of a gripper represents its ability to hold the object. This information can also be presented in the form of level curves giving a visual representation of the behavior of the gripper.

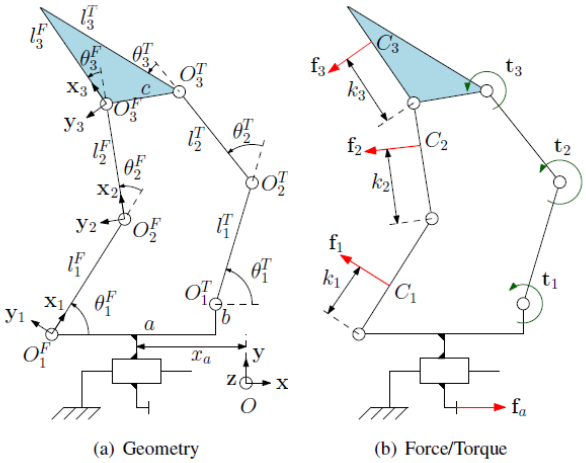

Figure 2.5 Parameters of the PaCoMe finger,
taken from (Birglen, 2015)

2.5 Previous Work

2.5.1 PaCoMe Finger

In (Birglen, 2009), the author presents a methodology that is able to generate thousands of self-adaptive robotic grippers that can be driven by linkages with two or three phalanges. The first part of the work is synthesizing potential kinematic architectures, and the second part is issuing proper actuation and passive element selection and location. However, in this work, an important design choice was left out in the discussion about the valid location(s) of the actuator(s) in the structure of the designs presented, which is the ground of the mechanism, or the base, as a replacement for the rotational actuator in the joints. This design choice is quite important because, as discussed in the previous section, the manufacturing and packaging industry still mostly relies on parallel grippers, which is a translational actuator with its axis perpendicular to the palm. They are reluctant to change their grippers for their operations because they have been using them for decades and it could be very costly to make the necessary adjustments for other grippers: different communication protocols, updating the robots' programs, providing adequate power, changing the adapter plates. So in order to address these challenges and to provide economical alternatives for the existing problem the author designed in (Birglen, 2015) self-

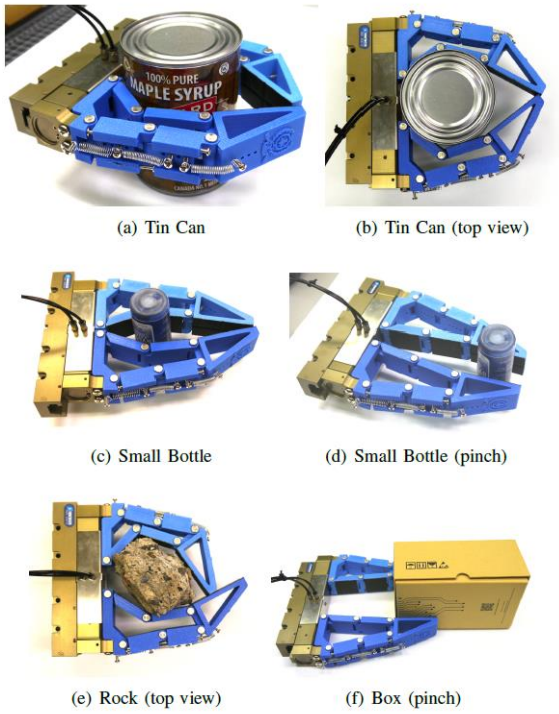

Figure 2.6 Grip tests performed by the PaCoMe finger, taken from (Birglen, 2015)

adaptive robotic gripper that can be actuated by moving its base in order for it to touch and grasp the object.

The finger is illustrated in Figure 2.5. The transmission linkage is an RRR chain or a simple planar motion generator. The prismatic joint at the bottom of the mechanism is added to model the parallel gripper on which the finger is attached. The design of the finger is based on a six-bar linkage and theoretically needs three actuators to fully constrain it. But instead of the actuators, springs are added between the proximal-intermediate and intermediate-distal phalanges while the third element is an actuator that can be placed in any joint of the transmission linkage. But for this mechanism, and in order to get rid of this actuator, three passive elements are used instead of two. The locations of the passive elements are chosen to be in the transmission linkage and the reason for this choice is to place them as far as possible from the objects to be seized to minimize possible interference (Birglen, 2015).

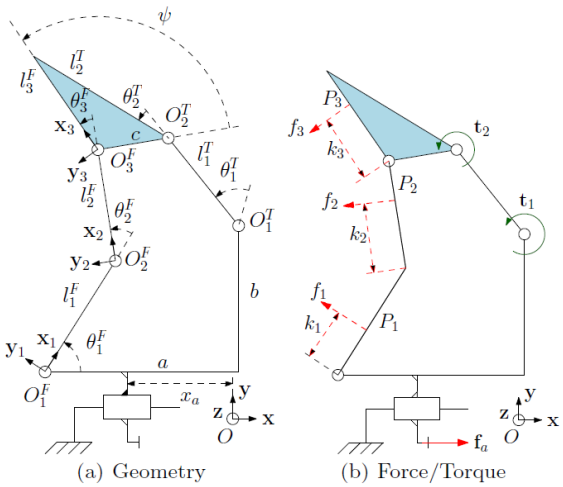

Figure 2.7 Parameters of the simplified finger based on a 5-bar mechanism, taken from (Birglen, 2019)

The prototype of the mechanism is illustrated in Figure 2.6 where the different grasps are demonstrated: cylinders with different diameters for the power grasps and the box for the pinch grasp. The gripper is able to effectively grasp different objects with strong and secure grasps. The prototype is named "PaCoMe", acronym for Passive Cord Mechanism, a nod to the Active Cord Mechanism (ACM) series: Prof. Hirose's snake-like robots. Indeed, both the phalanges and the transmission linkage of this mechanism can be seen as passive serial mechanisms with compliance in certain joints, which do not house any actuators and adapt themselves to the objects seized (Birglen, 2015).

2.5.2 Simplified five-bar finger

As mentioned before, the closing motion of the finger presented in (Birglen, 2015) is provided by an external prime mover, typically a traditional translational robotic gripper, and the finger itself is completely passive except for internal compliance. The contact forces of the mechanism can still be computed even though the finger has no actuators, as shown in (Birglen, 2015), and they are related to the input closing force of the gripper onto which the finger is attached. However, this finger was not designed for use with cobots but for applications requiring larger forces (an industrial translational gripper was used), resistance to collision, and the design had a major

safety issue with pinch points. The force of the industrial gripper used is sufficient to cause major damage or at least severe pain. So for this purpose, the author designed a new version of the passive finger in (Birglen, 2019),, taking into account all the specific aspects to cobots to ensure safety but also performance.

Having a transmission linkage providing full mobility to the phalanges is arguably not critical to ensure a successful grasp as evidenced by experimental results. A simplified design with only two revolute joints in the transmission linkage is thus proposed in (Birglen, 2019). The design of the mechanism is illustrated in Figure 2.7, it is actuated by a translational motion and wraps around a part with an arbitrary shape. The kinetostatic parameters associated with the linkage are also shown in Figure 2.7. The prismatic joint at the base of the mechanism is used to model the translational robotic gripper. When this joint is actuated, a contact between the proximal or intermediate phalanges and the object that is to be seized creates a movement in the phalanx joints $O_1^F, \dots, O_3^F$. These phalanges are initially constrained in the fully upright position by the springs in O_1^T and O_2^T . The finger then deforms to accommodate the shape of the object while the passive torques generate a compliant enveloping grasp (Birglen, 2019) .

A prototype of the finger was installed on a Baxter robot like shown in (Birglen, 2019). The fingers can be secured in many positions onto the adapters similarly as how the original fingers of Baxter's electric gripper can also be attached in many offset positions. The fingers were then operated by the usual software library provided by the manufacturer of the gripper without any modifications and they were found to work well for a variety of objects both in power and precision grasps. The translation range of the Baxter electric gripper dictates the range of motion of the fingers, namely 20mm for each finger, which makes the whole hand (gripper + fingers) able to seize objects in the range of 0 to 40mm. In practice, the minimal size of the objects as projected along the translational direction to ensure a safe and secure grasp was found to be around 5 mm. It should be noted that smaller objects such as a needle could still be efficiently seized with the fingers proposed here but using a pinch grasp similarly to the way humans seize small objects (Birglen, 2019).

CHAPTER 3 METHODOLOGY AND ORGANIZATION OF THE DOCUMENT

In order to evaluate the performance of simpler designs of self-adaptive fingers and using prismatic joints, four designs of 1-DOF fingers based on variations of four-bar mechanisms are studied in Chapter 4. The four fingers are different in terms of number of phalanges and whether or not there is a prismatic joint in the transmission linkage. A general kinetostatic analysis is first presented, in which a Jacobian and Transmission matrix were calculated for each finger and for each of the defined contact scenarios to compute the contact forces generated by the different designs. The mathematical models of the different mechanisms used for said calculations are presented as appendices. Appendix A calculates the expression of the Jacobian matrix for each mechanism, which is observed to be dependent on the number of phalanges of the finger; Appendix B calculates the velocity equations of the different links of the mechanisms used in the expressions of the Jacobian and the Transmission matrices; and Appendix C calculated the different parameters of the mechanisms used in the calculations function of the input angle.

The three fitness functions used for the optimization of the mechanisms are the percentage of the positive contact forces generated, the average value of the coefficient of variation of the contact forces, and the mechanical advantage of the mechanisms. These functions are commonly used for the optimization of self-adaptive fingers.

After using the fitness functions related to the generated contact forces by the fingers, the results of the optimization are shown and analysed. Although the optimization is focused exclusively on the generated forces and the enveloping capability of the fingers is not taken into consideration, it was noticed that fingers with rotational joints tend to have better enveloping grasps than the ones using a translational joint. Some possible improvements for the lower performing mechanisms in terms of enveloping grasps are then presented in Chapter 5 while adding the ability of pinch grasping.

CHAPTER 4 FORCE ANALYSIS OF MINIMAL SELF-ADAPTIVE FINGERS USING VARIATIONS OF FOUR-BAR LINKAGES

Fadi Nassar, Lionel Birglen

This article was submitted for publication in the journal Mechanical Sciences on July 19th 2021.

4.1 Abstract

This paper presents the design and optimization of four versions of self-adaptive, a.k.a underactuated, fingers based on four-bar linkages. These fingers are designed with the aim of being attached to and used with the same standard translational grippers as one finds in the manufacturing and packaging industries. Compared to previous works from the literature, this paper does not aim at making self-adaptive fingers more capable but simpler. It is often a common trend in research to focus on improving existing solutions by adding new parts, sensors, or actuators, often complexifying designs. On the other hand, the approach proposed here is to focus on making the design, of self-adaptive fingers in our case, as simple as possible and to analyse the resulting trade-off between complexity and performance. To this aim, the simplest one degree-of-freedom (DOF) linkage, namely a four-linkage, is used to build these fingers. However, it should be pointed out that if this work does consider a single four-bar linkage as the basic building block of the fingers, four variations of four-bar linkages are actually discussed including some with a prismatic joint. The ultimate purpose of this work is to evaluate whether simplest linkages for adaptive fingers can produce the same level of performance in terms of grasp forces as more complex designs. To this aim, a kinetostatic analysis of the four fingers is first presented. Then, these fingers are all numerically optimized considering various force-based metrics, and results are shown. Finally, the results and experimental prototypes are discussed.

4.2 Introduction

Self-adaptive, also known as underactuated (Birglen, Laliberté, & Gosselin, 2007), hands and fingers have been used in the last decade by both the research community and the industry as a compromise between complex anthropomorphic robotic hands and classical industrial grippers. Complex dexterous hands could require more than 3 fingers and 9 actuated degrees of freedom (DOF) to have desirable features such as accurate grasping and quick reaction (Hirose &

Umetani, 1978), while classical industrial grippers are made for simpler tasks that only require a motion produced by a one-DOF mechanism. Underactuated hands and fingers offer a simplicity in control not accessible to fully actuated designs since the number of actuators is smaller than the number of DOF. Often in an underactuated hand, a single actuator drives the whole hand. Additionally, underactuated hands are made not to depend on sensors for their operation while still having shape adaptation capabilities, i.e. being able to conform to a vast range of shapes of objects to grasp. Underactuated hands are also referred to as self-adaptive because of this property and to differentiate themselves from other applications of underactuation in robotics such as passive walkers. The first self-adaptive hand reported in the scientific literature was probably the Soft Gripper, introduced by Prof. Hirose (Hirose & Umetani, 1978), which was actuated by two wires and had two ten-phalanx fingers. Newer designs have been demonstrated since, most commonly showing anthropomorphic features (Li, Zhang, Zhang, Sun, & Chen, 2014), (Begoc, Krut, Dombre, Durand, & Pierrot, 2007), (Dollar & Howe, 2006), (Catalano, et al., 2012), (Abdeetedal & Mehrdad, 2018). Other robotic devices close to self-adaptive fingers have also been reported which are using structural compliance to achieve conformal grasps. They are referred to as soft hands and grippers. Amongst these soft grippers many can be found built using a particular design of bio-inspired fingers based on the Fin Ray Effect (FRE) (Crooks, Rozen-Levy, Trimmer, Rogers, & Messner, 2017), (Shan & Birglen, 2020) from which commercial products exist and are marketed by the company Festo.

Other commercial products exist for grasping hands either relying on underactuated mechanisms or soft robotics techniques. For instance, Robotiq's 2F-85 and 2F-140 Adaptive Grippers, RightHand Robotics RightPick, Soft Robotics Inc. mGrip, or the Gripper Company fingers are all commercially available products and appear quite successful in many markets. However, they are all new products while the manufacturing and packaging industry has been using pneumatic parallel grippers in their operations for a very long time and replacing them with any of these new designs is costly and time consuming. The only commercial product not requiring the replacement of the end-effectors in existing workcells are the FRE based fingers from Festo. Another similar solution addressing this problem was introduced in (Carpenter, Hatton, & Balasubramanian, 2014) in which an adaptive jaw was proposed that can be secured to and driven by a parallel gripper and consisting of three parallel hydraulic cylinders that are connected to a

Figure 4.1 PaCoMe fingers prototype on a Schunk gripper.

common local reservoir. By providing only an addition to a standard gripper, this solution eliminates the need to engineer a complex cable or linkage system to allow for finger adaptability. Yet another solution, proposed by the second author and inspired by the FRE, consists in designing a passively adaptive linkage to be attached to standard industrial grippers. When in contact with an object this linkage can deform in such a way that it provides an enveloping motion around the object it is in contact with. Actuation is thus provided by the motion of the gripper moving the base of the adaptive linkage, but the latter embeds no actuation or sensing element. In (Birglen, 2015), such a linkage named the PaCoMe finger was introduced: a three phalanx self-adaptive mechanical finger inspired by the FRE fingers but using rigid links instead of compliant ones. The PaCoMe finger has three degrees of freedom and consists in a 6-bar linkage in which specific joints embed a spring and a joint stopper. This finger was shown to produce stable enveloping and precision grasps while being attached to an off-the-shelf translational pneumatic gripper. An extension of this work was demonstrated in (Birglen, 2019) based on a slightly simpler linkage and specifically designed to match the requirements of collaborative robotics applications. This second finger design was based on the idea that a transmission linkage producing full mobility to the phalanges might not be mandatory to achieve a successful grasp. The simpler mechanism presented in (Birglen, 2019) was shown to be a valid alternative of the latter based on theoretical and experimental results. The same idea is also

shown in (Kok & Low, 2018) where one 2-DOF and then, one 1-DOF self-adaptive fingers are introduced to be used with industrial parallel grippers. Finally, another example of a self-adaptive finger with one DOF is presented in (Zheng & Zhang, 2019) where a four-bar mechanism along with an eccentric cam are used.

This paper aims at continuing and hopefully settling the discussion on this line of thought of producing the simplest self-adaptive finger possible by analyzing the performance of simple designs with only a single DOF. To this aim, four variations of self-adaptive designs are presented, all based on four-bar mechanisms. Two of these designs have two phalanges while the other two have three. Another uncommon feature of these designs is that two of them (one in each category: two- and three-phalanx fingers) use a prismatic joint. Prismatic joints in robotic fingers are not unheard of but they are uncommon as they significantly depart from anthropomorphic inspiration. However, for industrial grasping, the main market of the previously mentioned commercial products, anthropomorphic designs are not necessarily relevant.

4.3 Kinetostatic Analysis

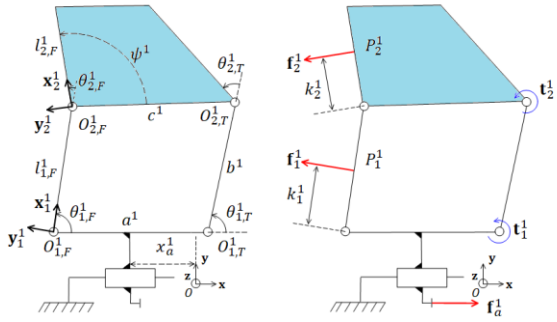

4.2 Parameters of finger #1

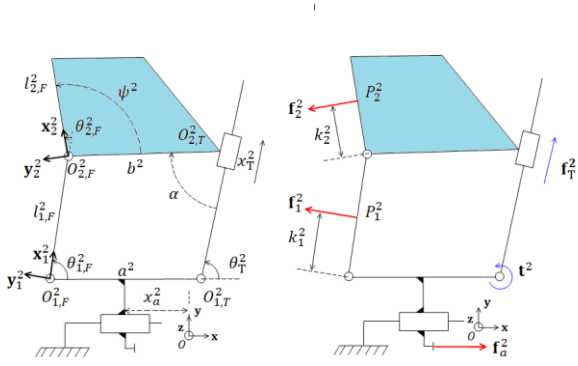

4.3 Parameters of finger #2

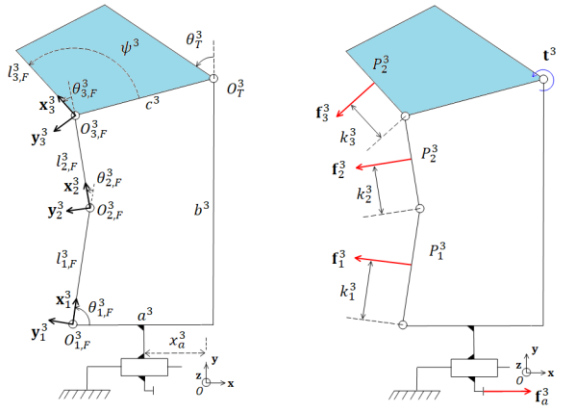

4.4 Parameters of finger #3

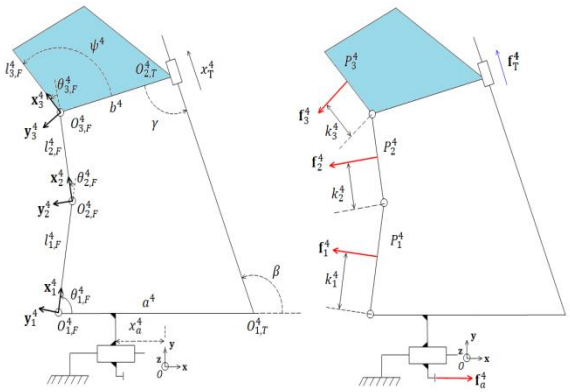

4.5 Parameters of finger #4

3D printed duplicate of the self-adaptive fingers presented in (Birglen, 2015) are shown in Figure 4.1 attached to a standard Schunk gripper. As mentioned before, these fingers are based on a six-bar linkage with revolute joints only and have three phalanges. These phalanges are constituted by the three consecutive binary links central to the hand and connected by three revolute joints. Two additional links and three revolute joints are used to form the transmission linkage of the finger at the outer side of each finger. This transmission linkage aims at avoiding constraining the DOF of the finger and ensuring that the resulting motion of the phalanges produces the desired shape-adaptation property for the mechanism. The revolute joints in the transmission linkage are equipped with springs with stoppers to fully constrain and preload the linkage when it is not subjected to external contact at the phalanges. The remaining link, i.e. the base of the linkage, is connected to the gripper movable jaws whose motion is one of a prismatic joint. Thus, the gripper acts a linear actuator for the fingers. A simplified design of this design was shown in (Birglen, 2019) in which the finger had only two DOF.

Following this effort in decreasing the number of DOF in self-adaptive fingers to simplify manufacturing and decrease cost even more, this paper proposes to reduce the DOF one step further to a single one. While there exist a multitude of one-DOF grippers proposed in the

literature, it should be made clear that the mechanisms proposed here are fundamentally different from these grippers. What is proposed here is a one-DOF mechanical finger to attach to a separate one-DOF gripper. Hence, the complete mechanism has two-DOF: one for the finger and one for the gripper. Contact forces are provided at the finger only and the gripper is creating the closing motion between the object and the mechanical finger. A zero-DOF finger could actually be made and would be a single rigid part. However, a zero-DOF finger would not be able to provide any shape adaptation. Hence, one DOF for an adaptive finger is the absolute minimal number of DOF one can use. Further highlighting the difference between the solution proposed here and simple articulated grippers, the mechanisms proposed here use two or three phalanges to envelope objects while articulated one-DOF grippers only create pinch grasps (a.k.a. precision grasps).

Mechanisms #1 and #2 considered in this paper have two phalanges and their geometry as well as their associated parameters are shown in Figure 4.2 and Figure 4.3. The transmission linkage of mechanism #1 is formed by two revolute joints in points $O_{1,T}^1$ and $O_{2,T}^1$ connecting a single link at the back of the finger. The transmission linkage of mechanism #2 is formed by one revolute and one prismatic joint, in point $O_{2,T}^2$ and of direction $\mathbf{x}_T^2$ respectively. Although only one spring on one joint of the transmission linkage in these two mechanisms is enough to fully constrain them (they have one DOF), two springs are considered in the model proposed below to be more general and establish the impact of these springs on the contact forces if needed. The input motion for the fingers is the translation along the axis $\mathbf{x}$ created by the gripper and with an associated force $\mathbf{f}_a$. Contact with an object can occur with either the proximal phalanx (points $O_{1,F}^1$-$O_{2,F}^1$) or distal phalanx (starting in point $O_{2,F}^1$ and of length $l_{2,F}^1$) thereby creating a contact forces $\mathbf{f}_1^1$ at point P_1^1 or $\mathbf{f}_2^1$ at point P_2^1 respectively.

Figure 4.4 and Figure 4.5 similarly illustrate the parameters of mechanisms #3 and #4. This time both linkages have three phalanges and thus, only a single joint remain for the transmission linkage (which in that sense is not “linkage” per se, being reduced to a joint). This remaining joint is either revolute for mechanism #3 or prismatic for mechanism #4. In both mechanisms, a spring is added to this joint to statically constrain the finger in the absence of a contact, similarly to mechanisms #1 and #2. In all cases, when the translational gripper modelled by the prismatic

joint at the base of the four mechanisms is driven, the finger is brought into contact with the object to be seized and this contact will cause a motion of the linkages in reaction to this contact assuming the input force of the gripper is sufficient to overcome friction at the contact point.

In order to be able to compare between these four fingers and the ones previously reported in the literature, two steps are required. As the performances of self-adaptive fingers are usually quantified by the magnitudes of the contact forces they produce, one must first establish these forces. Then, in a second time and to obtain a meaningful comparison, these fingers must be optimized with respect to these forces so the best fingers possible are used in the comparisons. Assuming that dynamic forces are negligible since the masses and inertias of the links are usually relatively small, one can use the virtual work principle to calculate these contact forces. The general form of the total virtual work for the fingers is:

$$\delta W^i = \mathbf{f}_a^{i\,T} \delta \mathbf{x}_a^i + \mathbf{f}_j^{i\,T} \delta \mathbf{y}_j^i + \mathbf{t}^{i\,T} \delta \boldsymbol{\theta}^{T\,i} \tag{4.1}$$

The index i in the previous equation is used to denote which one of the four mechanisms is being considered; for example, δW^1 is the virtual work of mechanism #1. Vector $\mathbf{f}_a^i = f_a^i \mathbf{x}$ is the force associated with the linear actuator at the base of mechanism i, translating along the x-axis. The infinitesimal motion of that base is $\delta \mathbf{x}_a^i = \delta x_a^i \, \mathbf{x}$. The contact forces at the jth phalanx of mechanism i is $\mathbf{f}_j^i$ and the virtual displacement in the direction of this contact force is $\delta \mathrm{y}_j^i$. The torques created by the various springs of the linkage are grouped in vector $\mathbf{t}^i$ and the infinitesimal relative rotation and/or displacement in the joint(s) of the transmission linkage are grouped in vector $\delta \boldsymbol{\theta}^{T\,i}$. Beside in the expression of this last vector, all other *"**T**"* in the previous equation (superscript) denotes the mathematical transpose operator. It should be noted that the expressions of $\mathbf{t}^i$ and $\delta \boldsymbol{\theta}^{T\,i}$ is different for each mechanism because of the differences in the transmission linkages and the number of springs, namely one has:

$$\mathbf{t}^1 = \begin{bmatrix} \mathrm{t}_1^1 \\ \mathrm{t}_2^1 \end{bmatrix} = \begin{bmatrix} -k_{r_1}{}^1 \left(\theta_{1,T}^1 - \theta_{1,T}{}_0^1 \right) \\ -k_{r_2}{}^1 \left(\theta_{2,T}^1 - \theta_{2,T}{}_0^1 \right) \end{bmatrix}, \qquad \boldsymbol{\theta}^{T\,1} = \begin{bmatrix} \theta_{1,T}^1 \\ \theta_{2,T}^1 \end{bmatrix}, \tag{4.2}$$

$$\mathbf{t}^2 = \begin{bmatrix} \mathrm{t}^2 \\ \mathrm{f}_T^2 \end{bmatrix} = \begin{bmatrix} -{k_r}_1^2\left(\theta_T^2 - {\theta_T}_0^2\right) \\ -{k_l}_2^2\left(x_T^2 - {x_T}_0^2\right) \end{bmatrix}, \qquad \boldsymbol{\theta}^{T\,2} = \begin{bmatrix} \theta_T^2 \\ x_T^2 \end{bmatrix}, \tag{4.3}$$

$$\mathbf{t}^3 = -{k_r}^3\left(\theta_T^3 - {\theta_T}_0^3\right)\mathbf{z}, \qquad \boldsymbol{\theta}^{T\,3} = \theta_T^3\mathbf{z}, \tag{4.4}$$

$$\mathbf{t}^4 = \mathbf{f}_T^4 = -{k_l}^4\left(x_T^4 - {x_T}_0^4\right)\mathbf{u}^4, \qquad \boldsymbol{\theta}^{T\,4} = x_T^4\mathbf{u}^4 \tag{4.5}$$

where ${k_r}_j^i$ and ${k_l}_j^i$ are the stiffnesses of the rotational and linear springs respectively that are used in the mechanisms. Angles and lengths $\theta_{j,T_0}^i, x_{T_0}^i$ are the initial values of the transmission linkage angles and displacements respectively when the force or torque in the springs is equal to zero, and finally $\mathbf{u}^4$ is a unitary vector along the axis of the prismatic joint of the finger if there is one.

All of the fingers discussed in this paper have one DOF and can therefore be constrained by a single contact. Therefore, two cases (contact scenarios) are possible for mechanisms #1 and #2 since they have two phalanges, and three contact scenarios are possible for mechanisms #3 and #4 since these have three phalanges. A contact scenario is defined as a situation with one contact point at one specific phalanx. For a contact scenario j (namely, at the jth phalanx counting from the base), the vector $\mathbf{f}_j^i$ models the contact force in mechanism i. These forces are considered normal to the surface of the phalanges (neglecting friction) and acting along a vector $\mathbf{y}_j^i$ with $j = 1{,}2$ for mechanisms #1 and #2, and $j = 1{,}2{,}3$ for mechanisms #3 and #4. Neglecting friction is unrealistic in practice but this hypothesis is often made in the literature, e.g. (Birglen, 2015), (Birglen, 2019) to yield the best mechanism possible from a kinematic perspective, i.e. without the help of friction during the grasp. Furthermore, friction does not affect the total squeezing force which is normal to the phalanges and of great importance to improve disturbance rejection and slippage prevention. Finally, the vector $\boldsymbol{\delta}\mathbf{y}_j^i$ is defined by:

$$\delta\mathbf{y}_j^i = \delta\mathbf{r}_{P_j^i}^T\mathbf{y}_j^i \tag{4.6}$$

where $\mathbf{r}_{P_j^i}$ is the vector from point $O_{j,F}^i$ to the contact point P_j^i which is at a distance k_j^i from the base of the corresponding phalanx. After equating the virtual work equation to zero in order to compute the contact forces at equilibrium, one obtains:

$$\begin{bmatrix} \mathbf{f}_a^i \\ \mathbf{f}_j^i \end{bmatrix} = -\left(\mathbf{J}_j^i\right)^{-T} \mathbf{T}_j^{iT} \mathbf{t}^i \tag{4.7}$$

where $\mathbf{J}_j^i$ is the grasp Jacobian matrix and $\mathbf{T}_j^i$ is the transmission matrix of the mechanism i for contact scenario j. These matrices will be calculated for each mechanism in the next sections.

4.3.1 Jacobian Matrix

By choosing the two DOF of the mechanisms (one for the finger and one for the actuation) as the translation x_a and the angle where the contact occurs $\theta_{j,F}^i$ in a specific contact scenario, the Jacobian matrix $\mathbf{J}_j^i$ can be defined for each mechanism for each contact scenario such that:

$$\begin{bmatrix} \delta x_a^i \\ \delta y_j^i \end{bmatrix} = \mathbf{J}_j^i \begin{bmatrix} \delta x_a^i \\ \delta \theta_{j,F}^i \end{bmatrix}. \tag{4.8}$$

Again, mechanisms #1 and #2 have two phalanges which means that there is only two contact scenarios, while mechanisms #3 and #4 have three contact scenarios since they have three phalanges. The Jacobian matrices can be calculated for each mechanism for each contact scenario by finding an expression of $\mathbf{y}_j^i$ expressed as a function of $\delta\theta_{j,F}^i$ and δx_a^i using basic geometrical relationships and taking the derivative of the latter. The results for all mechanisms and contact scenarios 1 and 2 (contact on the first two phalanges) are:

$$\mathbf{J}_1^i = \begin{bmatrix} 1 & 0 \\ -s_1^i & k_1^i \end{bmatrix}, \tag{4.9}$$

$$\mathbf{J}_2^i = \begin{bmatrix} 1 & 0 \\ -s_{12}^i & X^i\left(l_{1,F}^i c_2^i + k_2^i\right) + k_2^i \end{bmatrix}. \tag{4.10}$$

The last case, namely contact scenario 3 for mechanisms #3 and #4 yields:

$$\mathbf{J}_3^i = \begin{bmatrix} 1 & 0 \\ -s_{123}^i & Y^i\left(l_{1,F}^i c_{23}^i + l_{2,F}^i c_3^i + k_3^i\right) + Z^i\left(l_{2,F}^i c_3^i + k_3^i\right) + k_3^i \end{bmatrix}. \qquad (4.11)$$

In Eqs. (4.9) - (4.11) $s_{m..n}^i$ is a simplified notation for $\sin\left(\sum_{k=m}^n \theta_{k,F}^i\right)$ and $c_{m..n}^i$ for $\cos\left(\sum_{k=m}^n \theta_{k,F}^i\right)$, $l_{j,F}^i$ is the length of the phalanx j of mechanism i while X^i, Y^i, and Z^i are angular velocity ratios defined as follows:

$$X^i = \frac{\delta\theta_{1,F}^i}{\delta\theta_{2,F}^i}, \qquad Y^i = \frac{\delta\theta_{1,F}^i}{\delta\theta_{3,F}^i}, \qquad Z^i = \frac{\delta\theta_{2,F}^i}{\delta\theta_{3,F}^i}. \qquad (4.12)$$

These equations can be used to express the Jacobian matrix in Eq. (4.8) and the components of the latter depend on the geometry of each 4-bar mechanism which is indeed very different in each case since every finger has his unique combination of number of phalanges and the use or not of prismatic joints.

4.3.2 Transmission Matrix

The Transmission matrix $\mathbf{T}_j^i$ relates the displacements of the angles and/or distances of the joint(s) of the transmission linkage to the chosen DOFs in the Jacobian matrix for each mechanism. Its general form is thus:

$$\delta\boldsymbol{\theta}^{T^i} = \mathbf{T}_j^i \begin{bmatrix} \delta x_a^i \\ \delta\theta_{j,F}^i \end{bmatrix}. \qquad (4.13)$$

For mechanisms #1 and #2, the transmission linkage has two joints since it is formed by two rotational joints for mechanism #1 and one rotational and one prismatic for mechanism #2 so $\delta\boldsymbol{\theta}^{T^1}$ and $\delta\boldsymbol{\theta}^{T^2}$ are 1×2 vectors containing the displacements of the two angles $\theta_{1,T}^1$ and $\theta_{2,T}^1$ for the first, and the displacements of the angle θ_T^2 and the distance x_T^2 for the second one. $\mathbf{T}_j^1$ and $\mathbf{T}_j^2$ are then 2×2 matrices having zeroes in their first column and the velocity equations of the transmission linkage parameters for contact scenario j in their second column. For mechanism #1 one has:

$$\delta\boldsymbol{\theta}^{T\,1} = \begin{bmatrix} \delta\theta_{1,T}^{1} \\ \delta\theta_{2,T}^{1} \end{bmatrix} = \mathbf{T}_j^1 \begin{bmatrix} \delta {x_a}^1 \\ \delta\theta_{j,F}^{1} \end{bmatrix} \tag{4.14}$$

$$\mathbf{T}_j^1 = \begin{bmatrix} 0 & \frac{\delta\theta_{2,T}^{1}}{\delta\theta_{j,F}^{1}} \\ 0 & \frac{\delta\theta_{1,T}^{1}}{\delta\theta_{j,F}^{1}} \end{bmatrix} \qquad \text{For } j = 1,2 \tag{4.15}$$

For mechanism #2 these equations become:

$$\delta\boldsymbol{\theta}^{T\,2} = \begin{bmatrix} \delta\theta_{T}^{2} \\ \delta x_{T}^{2} \end{bmatrix} = \mathbf{T}_i^2 \begin{bmatrix} \delta {x_a}^2 \\ \delta\theta_{j,F}^{2} \end{bmatrix} \tag{4.16}$$

$$\mathbf{T}_j^2 = \begin{bmatrix} 0 & \frac{\delta\theta_{T}^{2}}{\delta\theta_{j,F}^{1}} \\ 0 & \frac{\delta x_{T}^{2}}{\delta\theta_{j,F}^{1}} \end{bmatrix} \qquad \text{For } j = 1,2 \tag{4.17}$$

With mechanisms #3 and #4, their transmission "linkage" has only a single joint, revolute for mechanism #3 and prismatic for mechanism #4 and therefore, the expressions are a bit simpler. In these cases $\delta\boldsymbol{\theta}^{T\,3}$and $\delta\boldsymbol{\theta}^{T\,4}$ actually become a one dimension vector, i.e. a scalar value, representing the displacements of the angle θ_T^3 and the distance x_T^4 respectively. Matrices $\mathbf{T}_i^3$ and $\mathbf{T}_i^4$ are then 1×2 vectors having zero as the first element and the velocity ratio of the transmission linkage joint to the selected DOF in contact scenario j as the second element. This gives for mechanism #3:

$$\delta\boldsymbol{\theta}^{T\,3} = \delta\theta_T^3 = \mathbf{T}_j^3 \begin{bmatrix} \delta {x_a}^3 \\ \delta\theta_{j,F}^{3} \end{bmatrix} \tag{4.18}$$

$$\mathbf{T}_j^3 = \begin{bmatrix} 0 & \frac{\delta\theta_{T}^{3}}{\delta\theta_{j,F}^{3}} \end{bmatrix} \qquad j = 1,2,3 \tag{4.19}$$

and for mechanism #4 one obtains:

$$\delta\boldsymbol{\theta}^{T^4} = \delta x_T^4 = \mathbf{T}_j^4 \begin{bmatrix} \delta x_a{}^4 \\ \delta\theta_{j,F}^4 \end{bmatrix} \tag{4.20}$$

$$\mathbf{T}_j^4 = \begin{bmatrix} 0 & \dfrac{\delta x_T^4}{\delta\theta_{j,F}^4} \end{bmatrix} \qquad j = 1,2,3 \tag{4.21}$$

4.4 Design Optimization

4.4.1 Fitness Functions and Variables

Once the contact force generated by a finger design can be calculated as described in the previous section, one can start the optimization process of these forces. The same fitness function needs to be used for the four mechanisms in order to have a standardized evaluation of their performances and this function must be as close as possible to the one used in the literature. In general, many different optimization criteria are used in the literature for underactuated robotic grippers (Kragten & Herder, 2010), but in the context of this work, three fitness functions were used:

1. the percentage of the positive contact forces generated,
2. the average value of the coefficient of variation of the contact forces,
3. and the mechanical advantage of the mechanisms.

It is known that underactuated and self-adaptive fingers do not always generate positive contact forces at all phalanges in all configurations and this is one of their main drawbacks. Generating a negative contact force means that the finger has to pull on the surface of the object to be seized, which is impossible in most cases, and will then eventually lose contact with the object after sliding along its surface, a phenomenon known as ejection. It is desirable to minimize the occurrence of these negative forces, and this is the reason why the first fitness function is used both here and in the literature. The associated metric of performance can be written:

$$\mu^i = \frac{1}{n^i}\sum_{j=1}^{n^i} \frac{\int_W k\left(\theta_{1,F}^i\right) d\theta_{1,F}^i}{\int_W d\theta_{1,F}^i} \tag{4.22}$$

where μ^i is dimensionless and its maximal value is 1, W is the workspace of the mechanism and is considered here to be in terms of the proximal phalanx angle range of motion since all the mechanisms have one DOF. The Kronecker symbol for the positiveness of the contact forces, $k(\theta_{1,F}^i)$, is equal to zero if the force $\mathbf{f}_j^i$ that constrains the finger in the configuration set by $\theta_{1,F}^i$ is positive, and equal to one otherwise. The scaling factor n^i is the number of phalanges of the considered finger, it is equal to two for mechanisms #1 and #2, and equal to three for mechanisms #3 and #4. This scaling ensure that the performance index stays between zero and one.

The second optimization criterion used in this paper is the average value of the coefficient of variation of the contact forces. The contact forces generated by the mechanism could be irregular even if they are always positive and this is detrimental to the objective of securing objects of vastly different shapes and sizes. It is more desirable to even out the generated forces in the workspace of the fingers in order to be able to apply a relatively constant pressure on the object to be seized whatever its geometry. The average value of the coefficient of variation can be defined mathematically as:

$$c_v^i = \frac{1}{n^i}\sum_{j=1}^{n^i}\frac{\int_W (1-k(\theta_{1,F}^i))(s^i/\bar{f}^i)d\theta_{1,F}^i}{\int_W d\theta_{1,F}^i} \tag{4.23}$$

where s^i is the standard deviation of the contact forces for a defined design of mechanism i and $\bar{f}^i$ is the average value of these forces. The same definition for the Kronecker symbol used in μ^i applies for c_v^i.

Finally, the third optimization criterion introduced here is the mechanical advantage of the mechanism. The forces generated by the fingers (while being positive and even with optimal coefficient of variation, i.e. of close magnitudes) could still be significantly weaker that the actuation force provided by the gripper. This decrease of the contact forces compared to the gripper's is detrimental if fine force control is required and also strongly weakens the grasp as one potentially "loses" a significant part of the actuation effort. This phenomenon was identified as one of the major weaknesses of FRE fingers in (Carpenter, Hatton, & Balasubramanian, 2014)

and can cause slippage of the object from the hand at high speed pick and place. Quantifying the mechanical advantage of a self-adaptive finger gives an idea on the general efficiency of the fingers since it is in a sense the ratio between the input (gripper) and the output (finger) forces. Ideally, the contact force generated by the finger onto an object should be equal to the closing force delivered by the translational actuator at the base to maximize the efficiency. The general mathematical equation for the mechanical advantage can therefore be written as:

$$m_a = \frac{f_j^i}{f_{a_j}^{\ i}} \tag{4.24}$$

To integrate this equation into the optimization process, the first step is to normalize the values of this mechanical advantage to get values ranging from 0 to 1. The second step is to calculate its average for each contact scenario j, and finally, to calculate the average of 1 minus the value calculated in step 2 (the optimal value for the mechanical advantage is 1 in the previous equation but for optimization we need to minimize performance metrics). The mathematical equation for the mechanical advantage performance index used in this paper thus becomes:

$$m_{a_N}{}_j^{\ i} = \frac{1}{n^i}\sum_{j=1}^{n^i} \frac{1 - \int_W \frac{\left(\frac{f_j^i}{f_{a_j}^{\ i}}\right) - \left(\frac{f_j^i}{f_{a_j}^{\ i}}\right)_{min}}{\left(\left(\frac{f_j^i}{f_{a_j}^{\ i}}\right)_{max} - \left(\frac{f_j^i}{f_{a_j}^{\ i}}\right)_{min}\right)} d\theta_{1,F}^i}{\int_W d\theta_{1,F}^i}. \tag{4.25}$$

With all the mechanisms in this paper and again similarly to what is found in the literature, the position of the contact force on each phalanx k_j^i is assumed to be mid-phalanx. The workspace W is chosen as:

$$\frac{\pi}{4} \leq \theta_{1,F}^i \leq \frac{\pi}{2} \tag{4.26}$$

and one can calculate all the other angles and lengths of the four-bar linkages using textbook formulae for this range of input angles. The constants during the optimization are the lengths of

the phalanges $l_{j,F}^{i}$ which are taken to be unitary and the stiffnesses of the springs used in the transmission linkage, also taken to be unitary. For finger #4, b^4 is taken to be unitary and γ is taken to be $\frac{\pi}{2}$ since these geometrical parameters do not affect the values of the obtained generated contact forces of the finger and including them in the optimization process would be redundant. The remaining geometrical parameters to be optimized are presented in Table 4.1 Geometrical parameters of the fingers to be optimized. To optimize these mechanisms, a genetic algorithm from a commercial software package is used. All the values of the parameters in each generation including the initial population are constrained in a range of values delimited by a lower and upper bound shown in Table 4.1 Geometrical parameters of the fingers to be optimized. The upper bound for all the dimensions is set to be 3 to maintain a reasonable level of compactness for the fingers. The maximal number of generations is set to 1,000 and the algorithm also stops if the average relative change in the best fitness function value over 500 generations is less than or equal to its standard tolerance. Convergence is generally achieved within 700 generations with slight differences for each finger. The genetic algorithm minimizes a single value for each finger, f^i, which is a combination of the three fitness functions described above. The weights for the functions are distributed as follows: 50% for the mechanical advantage, 40% for the percentage of the positive contact forces, and 10% for the average value of the coefficient of variation of the contact forces. The choice of these weights is based on the importance and impact of each optimization function on the optimized geometrical parameters of the mechanisms.

Table 4.1 Geometrical parameters of the fingers to be optimized

Finger	Parameters	Ranges	Description
#1	$\begin{cases} a^1 \\ b^1 \\ c^1 \\ \psi^1 \end{cases}$	$\begin{cases} [0;3] \\ [0;3] \\ [0;3] \\ [0;\pi] \end{cases}$	
#2	$\begin{cases} a^2 \\ b^2 \\ \alpha \\ \psi^2 \end{cases}$	$\begin{cases} [0;3] \\ [0;3] \\ [0;\pi] \\ [0;\pi] \end{cases}$	

#3	$\begin{cases} a^3 \\ b^3 \\ c^3 \\ \psi^3 \end{cases}$	$\begin{cases} [0;3] \\ [2;3] \\ [0;3] \\ [0;\pi] \end{cases}$	The lower bound of b^3 is the sum of the lengths of the two phalanges in their upright position.
#4	$\begin{cases} a^4 \\ \beta \\ \psi^4 \end{cases}$	$\begin{cases} [0;3] \\ [\frac{\pi}{2};\pi] \\ [0;\pi] \end{cases}$	The lower bound of β is $\frac{\pi}{2}$ for better compactness of the geometry of the finger.

4.4.2 Results and discussions

Table 4.2 presents the values of the optimized parameters and the values of the optimization functions for all the fingers. All the optimized fingers generate positive contact forces exclusively throughout their workspaces since the value of μ^i is zero for all the mechanisms. This means that no finger will have to pull on the surface of the object to be seized in all their possible configurations. In terms of the average value of the coefficient of variation of the contact forces, it is seen that the fingers with two phalanges have better performance than the fingers with three phalanges. Indeed, finger #1 has the lowest value with $c_v^1 = 0.138$, followed by finger #2, then finger #4, and last finger #3 with $c_v^3 = 0.7279$. Intuitively, this statement seems to make sense as two-phalanx fingers have fewer potential cases of generated forces to maintain the finger in a specific configuration (they have two possible scenarios for one configuration while the three-phalanx fingers have three) and it becomes harder to keep all the generated forces close in terms of magnitude when the number of possible contact points increases. What is more interesting is the quantification of this effect and comparison between fingers with the same number of phalanges still hold. As for the mechanical advantage of the fingers, it is seen that finger #1 has the best value with $m_a^1 = 0.2121$. This means that, out of the four fingers, finger #1 is able to transmit the input force from the linear actuator to the object with the least amount of reduction.

As for the forces, plotted in Figure 4.7a) for finger #1, $\mathbf{f}_1^1$ and $\mathbf{f}_2^1$ have relatively close values for any input angle, meaning that for a specific pose of that finger, the generated force from contact at the proximal phalanx has approximately the same magnitude as one generated at the distal phalanx. The only notable deviation is within the range $60° \leq \theta_{1,F}^1 \leq 70°$ where $\mathbf{f}_2^1$ is slightly greater by a margin of 0.1N which might be considered small but is a fair amount considering that the maximal value of both generated forces in this plot is 1N. One can also notice from the

Table 4.2 Values of the optimized parameters and the optimization functions

	Finger #1	Finger #2	Finger #3	Finger #4
Performance Metrics				
μ^i	0	0	0	0
c_v^i	0.138	0.2319	0.7279	0.1987
m_a^i	0.2121	0.2931	0.3432	0.4313
f^i	0.1198	0.1697	0.2443	0.2355
Optimized Parameters				
a^i	1.77	2.41	1.44	1.79
b^i	2.45	1.85	2.88	1
c^i	1.59		1.64	
ψ^i	0.64	1.77	0.94	2.38
α		2.34		
β				2.02
γ				1.14

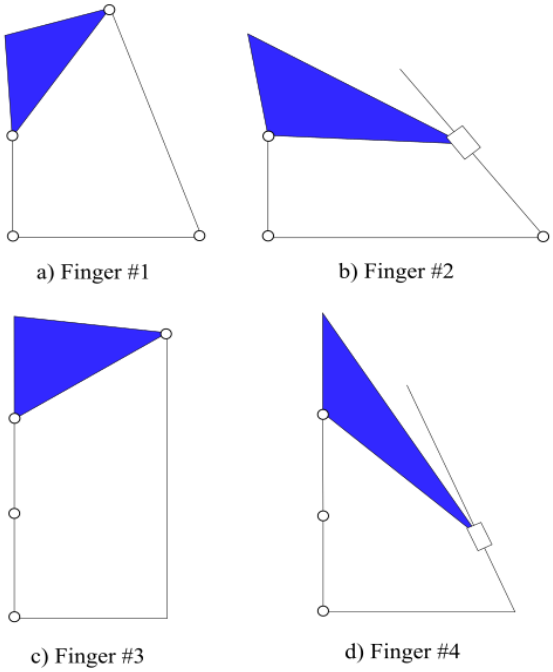

Figure 4.6 Geometry of the optimized fingers

plot in Figure 4.7b) that the actuation force of the translational gripper is transmitted in a different manner to the contact point on each phalanx. Indeed, even though both plots have a quasi linear allure, the slope of the graph corresponding to the force $\mathbf{f}_1^1$ is greater than that of the one corresponding to $\mathbf{f}_2^1$, meaning that the same input force generate a noticeably greater contact force on the proximal phalanx (0.7N) than on the distal phalanx (0.5N) and that phenomenon becomes more and more apparent for an actuation force $\mathbf{f}_a^1 > 0.2N$, or for an input angle $\theta_{1,F}^1 > 50°$.

For finger #2, it can be seen in Figure 4.7c) that, for this finger also, the generated contact force on the proximal phalanx $\mathbf{f}_1^2$ that constrains the mechanism in a certain configuration is very close in value to the generated contact force on the distal phalanx $\mathbf{f}_2^2$ that constrains the mechanism in the exact same configuration only in the part of the workspace where $\theta_{1,F}^2 \geq 55°$. For the values $45° \leq \theta_{1,F}^2 < 55°$ where the maximum forces are found, the value of the force $\mathbf{f}_2^2$ is greater than that of $\mathbf{f}_1^2$ (the overall maximal value of $\mathbf{f}_2^2$ is 4N greater than that of $\mathbf{f}_1^2$). Figure 4.7d) shows a quasi linear relationship between $\mathbf{f}_2^2$ and $\mathbf{f}_a^2$ with a slope approximately equal to one, and a

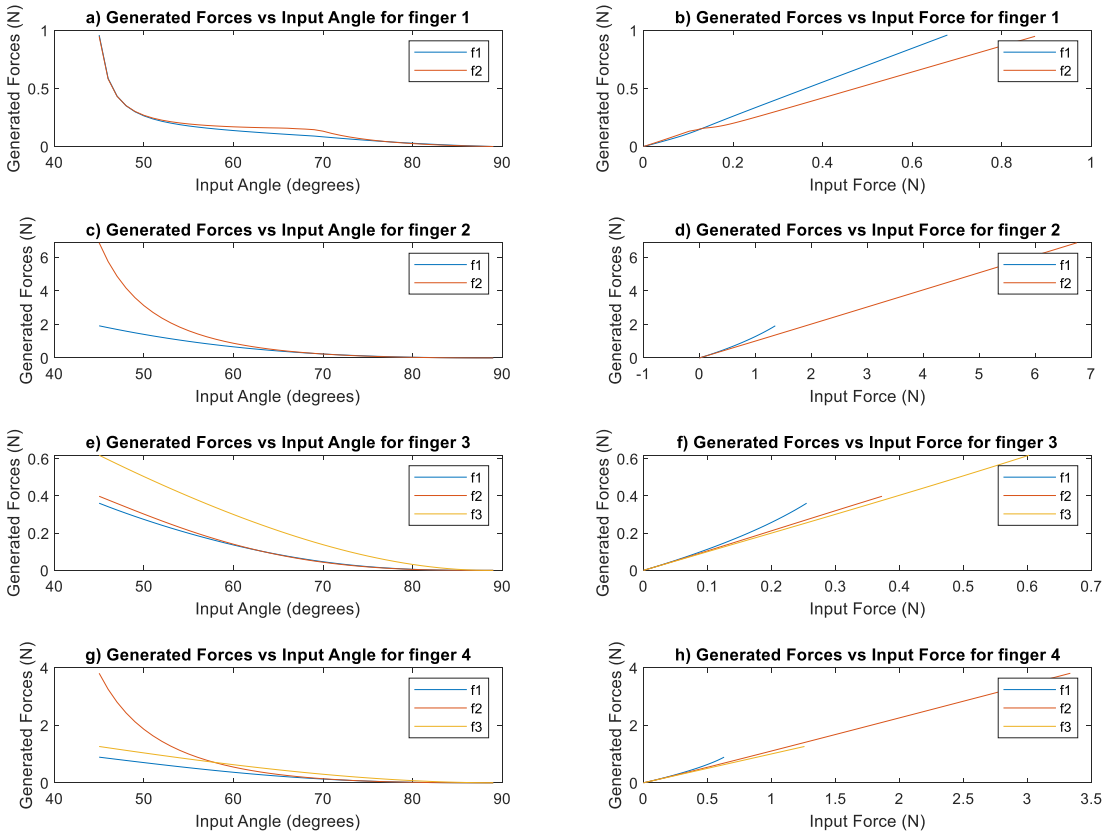

Figure 4.7 Plots of the generated forces function of the input angle and the input force for the four fingers

different, not as linear plot for $\mathbf{f}_1^2 = f(\mathbf{f}_a^2)$. For this mechanism also, the transmission of the actuation force to the contact points of the phalanges is better for the proximal phalanx since its plot in its entirety is above the one for the distal phalanx in the y-axis of the graph, meaning that for a same input force, the output force is greater in the proximal phalanx than at the distal one.

For finger #3, one can divide the workspace into two parts based on the plot shown in Figure 4.7e): for $45° \leq \theta_{1,F}^3 < 70°$, the valued of the generated contact force on the distal phalanx $\mathbf{f}_3^3$ to maintain the finger in a specific configuration is less than these of the generated forces on the proximal and intermediate phalanges $\mathbf{f}_1^3$ and $\mathbf{f}_2^3$ which are relatively close to each other in the same workspace range. For $80° < \theta_{1,F}^3 \leq 90°$, all of the contact forces in all the phalanges have very close values for a specific pose. As seen in Figure 4.7f), the input force delivered by

the translational motor is distributed in a relatively even manner among the phalanges since the values of the generated forces in each contact scenario (meaning in each of the proximal, intermediate, or distal phalanx contact) are close for the same input force $\mathbf{f}_a^3$. It should also be pointed out that this finger has the lowest maximal values for both the generated contact forces $\mathbf{f}_1^3$ (0.35N), $\mathbf{f}_2^3$ (0.4N), and $\mathbf{f}_3^3$ (0.6N) and the actuation force in the base $\mathbf{f}_a^3$ (0.6N), and that is because the transmission angle θ_T^3 doesn't change much throughout the workspace hence the finger is not generating an important torque in the spring of the corresponding joint. This issue could be solved by simply increasing the stiffness of the spring in the joint in the transmission linkage, or even by letting the finger go beyond its initial workspace ($\theta_{1,F}^3 < 45°$) in order for it to reach a singularity where the links $O_{2,F}^3 O_{3,F}^3$ and $O_{3,F}^3 O_{\mathrm{T}}^3$ become aligned and then, the mechanism will not be able to move anymore, so the output forces could then be increased by the actuation force in the translational actuator.

Finally, for finger #4 Figure 4.7g) demonstrates that all the phalanges generate contact forces that have very close values when $\theta_{1,F}^4 \geq 60°$ to constrain the mechanism in a specific configuration. But when $45° \leq \theta_{1,F}^4 < 60°$, the force generated by the intermediate phalanx $\mathbf{f}_2^4$ is greater than these generated by the proximal and distal phalanges $\mathbf{f}_1^4$ and $\mathbf{f}_3^4$ which in turn, have close values for the same configuration of the finger. In Figure 4.7h) it can be seen that the intermediate phalanx has the ability to generate much greater forces than the proximal and distal phalanges. Indeed, the maximum value for $\mathbf{f}_2^4$ in the workspace of the finger is 4N for and input force of 3.5N, while the maximum generated forces by the proximal and distal phalanges are 1N each for an input force of 0.6N and 1.2N respectively and that is due to the geometry of the finger and the difficulty to transmit a force acting on the intermediate phalanx to cause a sliding in the joint of the transmission linkage.

Now for the comparison with more complex linkages. If one looks at (Birglen, 2019), the percentage of the workspace corresponding to fully positive contact forces is reported to reach 9.7% depending on where the springs are located in the transmission linkage. A compliance in all joints of the latter, as used in this work, would give only 5.9%. For this finger, the average coefficient of variations of the contact forces is 0.73. Considering the second reference design proposed in (Kok & Low, 2018), a value of 7% is reported for the positive contact force

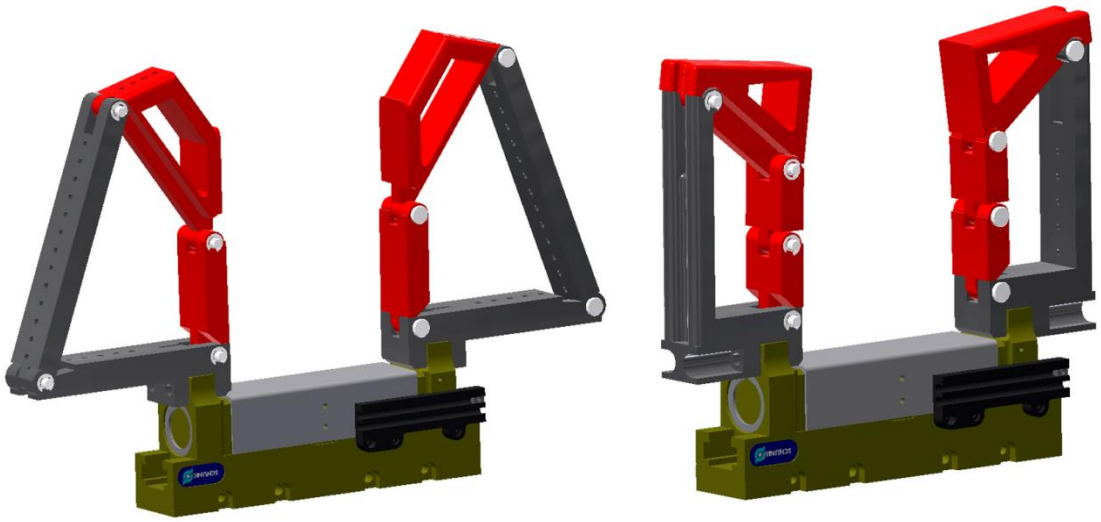

Figure 4.8 CAD models for the optimal designs of the fingers with only rotational joints

workspace. For the fingers presented in this paper, a percentage of positive contact forces in the workspace of 100% is achieved, whether the finger has two or three phalanges, or with a prismatic joint in the transmission linkage or not. Therefore, from this metric there seems to be a clear advantage to use simpler linkages while the resulting coefficient of variation seems of similar value for fingers with the same number of phalanges. The average coefficient of variations of the contact forces and the mechanical advantage in the 1-DOF fingers is seen to be negatively impacted by increasing the number of phalanges. The three-phalanx finger having a prismatic joint shows a better value for the average coefficient of variations of the contact forces when compared to the other three-phalanx finger but has a worse mechanical advantage.

4.5 Conclusion

This paper presented four different designs of self-adaptive mechanical fingers that can be actuated by the standard translational gripper used in the industry to transform this gripper into an underactuated hand and add shape-adaptability properties to the commonly found monolithic jaws used in the industry. The designs are simple in terms of kinematics when compared to previous prototypes from the literature since all of them are based on variations of four-bar mechanisms and have only one degree of freedom. Prismatic joints were also considered in two of these four fingers which is uncommon in artificial fingers, even industrial ones. A general

kinetostatic analysis was first presented, in which a Jacobian and Transmission matrix were calculated for each finger and for each of the defined contact scenarios to compute the contact forces generated by the different designs. Then, optimization criteria were discussed for the evaluation of the performances of the fingers. The three optimization functions used in this paper, namely the percentage of the positive contact forces generated by the mechanisms, the average value of the coefficient of variation of the contact forces, and the mechanical advantage of the mechanisms, gave a better understanding on the magnitude and variations of the generated contact forces between different phalanges. Although the mechanisms are simple in terms of geometry, their performances can be considered at least comparable with other prototypes with full mobility or even better. However, it should be noted that the optimization was focused exclusively on the generated forces and the enveloping capability of the fingers was not taken into consideration, and simulations show that fingers with rotational joints tend to have better enveloping grasps than the ones using a translational joint. This does not mean that using a prismatic joint in underactuated fingers will definitely lead to poor enveloping grasps.

The same finger could give different results with the appropriate design changes that can be done in future works. For instance, the ability to generate enveloping grasps can be considered in the optimization, or the original design of the fingers can be modified, i.e. combining one rotational with one translational joint for instance with finger #2. Future works can also include varying the different weights of the optimization functions and experimentally validating the effectiveness of the optimal designs presented in this work, see Figure 4.8.

CHAPTER 5 GENERAL DISCUSSIONS

As discussed in section 2.4.1, there is little control over the behavior of a self-adaptive finger after completing its design because not every one of its degrees of freedom is controlled independently. Thus, the characteristics of the grasp, depend either on the object to be seized, or on the geometry of the transmission linkage. In this Chapter, it is desired to potentially improve the quality of these characteristics for the 1-DOF self-adaptive fingers with prismatic joints introduced in Chapter 4 by proposing new geometries for their transmission linkages.

Self-adaptive fingers having 1-DOF have generally simple geometries, and subsequently, an even simpler control. Indeed, an on/off command for the single linear actuator, and if needed, the processing of the information coming from a single distance sensor are more than enough for these grippers to reach their full potential. What is proposed here is using the complexity of the control of the robotic arm on which this gripper is attached to push the limits of their potential caused by simple geometry. Of course if the control of the robotic arm is complex, then the arm itself is complex, either by its geometry or its number of actuators and sensors and can achieve complex tasks with a higher precision.

By modifying the geometry of the 1-DOF finger to make the grasp type of the finger change according to the location of the contact point with the object, the precision of the robotic arm can be used for the purpose of the gripper. The robot will have the ability to switch between enveloping and pinch grasps by simply positioning the gripper around the object accordingly. For this reason, two geometry designs are proposed for the finger having two phalanges and one design for the one having three.

It should be noted that a kinetostatic analysis was not developed for the designs presented below to get an accurate idea about their generated forces, but they should be close in value, direction, and variation to the ones of the generated forces in the mechanisms presented in Chapter 5 It is still essential to develop a mathematical model for these mechanisms to better understand them and be able to generate more optimized versions.

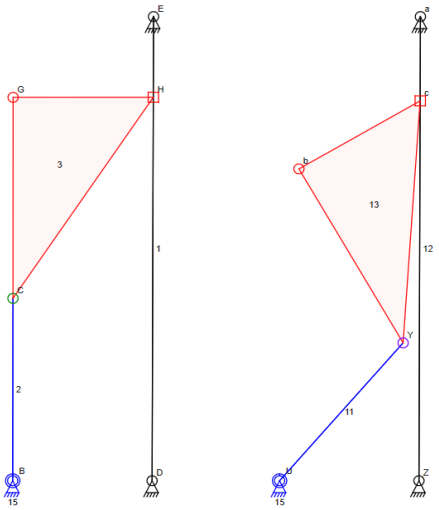

Figure 5.1 New design for the two-phalanx finger with a prismatic joint

5.1 Two-phalanx finger

The two-phalanx self-adaptive finger that used a prismatic joint presented in Chapter 4 is based on a variation of a four-bar mechanism called inverted slider-crank. In this mechanism, the axis of the prismatic joint is connected to the base with a rotational joint. What is proposed here is removing the rotational joint from the base of the axis of the prismatic joint, which will make this axis fixed, and add it on the same point of the translation. This will transform the inverted slider-crank into a normal one, as seen in Figure 2.2.

In general, the transmission of movements from rotation to translation, or vice versa, is smoother and more natural in standard slider-crank mechanisms than in inverted ones. The changes in the transmission linkage of this finger can be seen Figure 5.1 where the initial and final configurations of the finger are shown, in a workspace similar to the one used in Chapter 4. In terms of link dimensions, the new proposed design is more compact than the previous one and can achieve nearly the same enveloping grasp, if not a better one. It could at least be noted that this design has a better potential at generating positive forces since contact forces on both phalanges can be assimilated to a clockwise angular actuation at the base of the proximal

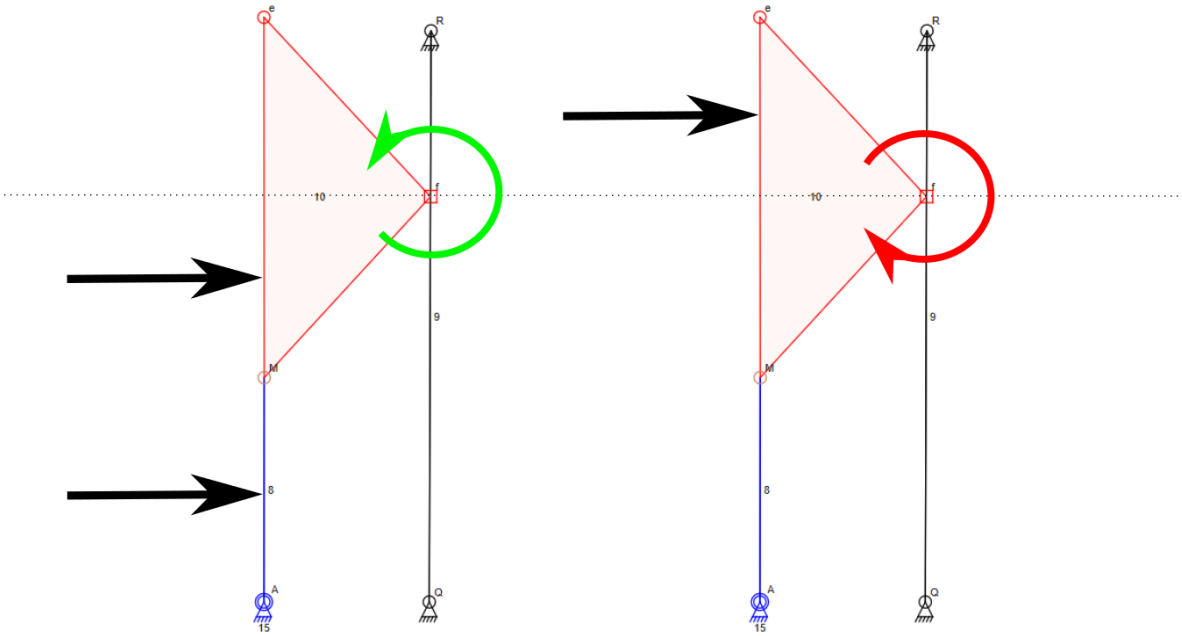

Figure 5.2 Mechanical stopper preventing the rotation of the distal phalanx in the clockwise direction

phalanx, meaning that the finger won't have to pull on the surface of the object to grasp in order for it to move.

Another similar design can have the same functionality of enveloping grasps, but also can achieve pinch grasping depending on the location of the contact point with the object to grasp. As seen in Figure 5.2, the location of the prismatic joint is in the middle of the distal phalanx, making the location of the contact point a deciding factor for the type of grasp. By placing a mechanical stopper in the rotational joint of the transmission linkage that only prevents the clockwise rotation of the joint, any movement generated by external forces whose location is above the prismatic joint in the initial configuration of the mechanism (the dotted line in Figure 5.2) will be prevented, since these forces can only cause a clockwise rotation in the rotational joint. Any other force below the dotted line will cause a normal motion of the linkage making the enveloping grasp possible just like the design seen in Figure 5.1.

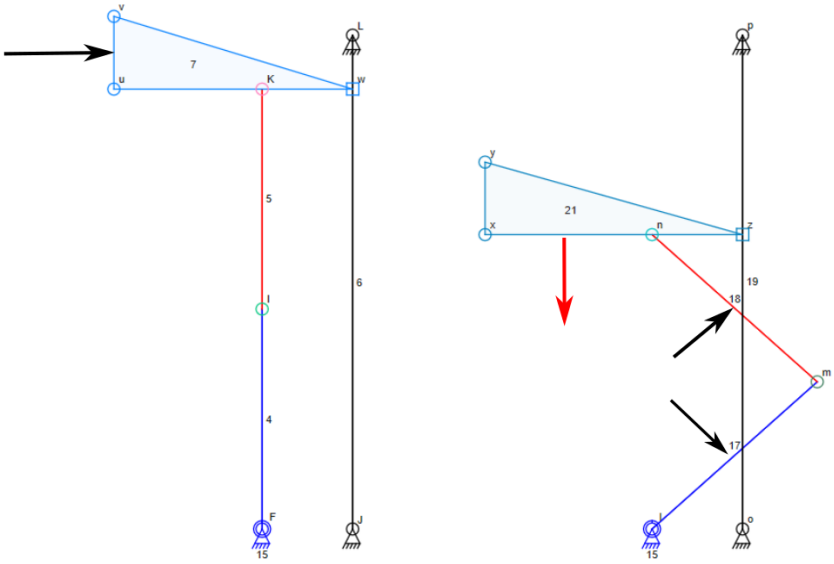

Figure 5.3 New design for the three-phalanx finger with a prismatic joint

5.2 Three-phalanx finger

For the three-phalanx finger, the design shown in Figure 5.3 is proposed. This design can also perform both enveloping and pinch grasps depending on the contact points with the object. If the contact with the object is with the proximal or intermediate phalanges, the grasp is an enveloping one and the generated forces are positive. The distal phalanx in this case applies vertical pressure on the object to get a better hold of it. This vertical force is shown in the right side of Figure 5.3. This same finger can perform a pinch grasp when the contact point with the object is on the distal phalanx like shown in the left side of Figure 5.3. In this case, the force will remain horizontal since the distal phalanx can only translate along the axis of the prismatic joint in the transmission linkage and therefore cannot rotate and change its orientation and subsequently that of the force. A horizontal force will not cause motion in the linkage since it is perpendicular to the axis of the prismatic joint which will give the ability of pinch grasping to this finger.

For this finger, and because of the shape of the distal phalanx, the type of objects it can grasp has limitations on its dimensions. If one assimilates the shape of the object in the plane to a rectangle,

its length has to be smaller than the distance between the base and the distal phalanx. And for its width, it has to be greater than double the horizontal length of the distal phalanx when the length is at its allowed maximum so that the two fingers performing the enveloping grasp don't collide. Since this is a 1-DOF mechanism, each elevation of the distal phalanx is assimilated to a single value of the input angle. This means that it is most likely that the finger reaches a fully constrained position where the distal phalanx doesn't touch the object. A solution to this problem would be to increase the number of phalanges between the base and the distal phalanx, and consequently increase the number of springs between the different to keep the finger constrained in an upright position when it is not in contact with the object.

CHAPTER 6 CONCLUSION

This research falls in the framework of research on self-adaptive grippers done in the robotics lab of École Polytechnique de Montréal. In order to evaluate the generated forces of simpler designs of self-adaptive fingers actuated by a linear motion in the base and with prismatic joints, four designs of 1-DOF fingers based on variations of four-bar mechanisms are analysed and discussed. Each one of these designs has a unique combination of number of phalanges (two or three) and presence/absence of a prismatic joint in the transmission linkage.

A general kinetostatic analysis was developed for each finger to compute the contact forces generated by the different designs. Then, the three optimization functions used in this paper, namely the percentage of the positive contact forces generated by the mechanisms, the average value of the coefficient of variation of the contact forces, and the mechanical advantage of the mechanisms, were discussed for the evaluation of the performances of the fingers . The result was that although the mechanisms are simple in terms of geometry, their performances can be considered at least comparable with other prototypes with full mobility or even better especially for the percentage of positive contact forces generated. It should be noted however that although the optimization was focused exclusively on the generated forces and the enveloping capability of the fingers was not taken into consideration, simulations show that fingers with rotational joints tend to have better enveloping grasps than the ones using a translational joint. For this reason, three other designs for the geometries of the fingers using prismatic joints were proposed to try and improve their functionality.

The next step for this line of work would be to generate a mathematical model for the new designs of the fingers using a prismatic joint by developing a kinetostatic analysis and implementing optimization criteria to the generated contact forces while taking the enveloping grasp into consideration, and to experimentally validate the effectiveness of all the optimal designs presented in this work.

REFERENCES

Abdeetedal, M., & Mehrdad, R. K. (2018). Grasp and stress analysis of an underactuated finger for proprioceptive tactile sensing. *IEEE/ASME Transaction on Mechatronics 23.4*(23.4), 1619-1629.

Almestiri, S. M., Murray, A. P., Myszka, D. H., & Wampler, C. W. (2016). Singularity traces of single degree-of-freedom planar linkages that include prismatic and revolute joints. *Journal of Mechanisms and Robotics 8*, 051003.

Bégoc, V., Durand, C., Krut, S., Dombre, E., & Pierrot, F. (2006). On the form-closure capability of robotic underactuated hands. *9th International Conference on Control, Automation, Robotics and Vision*, (pp. 1–8). Singapore, Singapore.

Begoc, V., Krut, S., Dombre, E., Durand, C., & Pierrot, F. (2007). Mechanical design of a new pneumatically driven underactuated hand. *Proceedings 2007 IEEE International Conference on Robotics and Automation.* IEEE.

Begoc, V., Krut, S., Dombre, E., Durand, C., & Pierrot, F. (2007). Mechanical design of a new pneumatically driven underactuated hand. *Proceedings 2007 IEEE International Conference on Robotics and Automation*, (pp. 927–933).

Birglen, L. (2009). The synthesis of linkage-driven self-adaptive fingers. *ASME Journal of Mechanisms and Robotics*.

Birglen, L. (2015). Enhancing Versatility and Safety of Industrial Grippers with Adaptive Robotic Fingers. *2015 IEEE/RSJ international conference on intelligent robots and systems (IROS)*, pp. 2911-2916.

Birglen, L. (2019). Design of a partially-coupled self-adaptive robotic finger optimized for collaborative robots. *Autonomous Robots 43.2*(43.2), 523-538.

Birglen, L., & Gosselin, C. M. (2003). On the force capability of underactuated fingers. *2003 IEEE International Conference on Robotics and Automation (Cat. No. 03CH37422)*, (pp. 1139–1145). Taipei, Taiwan.

Birglen, L., & Gosselin., C. M. (2006). Optimally unstable underactuated gripper: synthesis and applications. *International Design Engineering Technical Conferences and Computers and Information in Engineering Conference vol. 42568*, (pp. 3-11).

Birglen, L., & Herbecq, F. (2009). Self-adaptive compliant grippers capable of pinch preshaping. *International Design Engineering Technical Conferences and Computers and Information in Engineering Conference*, (pp. 249-257).

Birglen, L., Laliberté, T., & Gosselin, C. M. (2007). *Underactuated Robotic Hands.* Springer.

Birglen, L., Laliberté, T., & Gosselin, C. M. (2007). Underactuated robotic hands, Vol. 40. *Springer*.

Boudreault, E., & Gosselin, C. M. (2006). Design of sub-centimetre underactuated compliant grippers. *International Design Engineering Technical Conferences and Computers and Information in Engineering Conference*, (pp. 119-127). Philadelphia, PA, USA.

Boudreault, E., & Gosselin, C. M. (2006). Design of sub-centimetre underactuated compliant grippers. *International Design Engineering Technical Conferences and Computers and Information in Engineering Conference*, 119-127.

Carpenter, R., Hatton, R., & Balasubramanian, R. (2014). Comparison of contact capabilities for underactuated parallel jaw grippers for use on industrial robots. *International Design Engineering Technical Conferences and Computers and Information in Engineering Conference, Vol. 46377.* American Society of Mechanical Engineers.

Catalano, M. G., Grioli, G., Serio, A., Farnioli, E., Piazza, C., & Bicchi, A. (2012). Adaptive synergies for a humanoid robot hand. *2012 12th IEEE-RAS International Conference on Humanoid Robots (Humanoids 2012)* (pp. 7-14). Humanoid Robots (Humanoids).

Ceccarelli, M., Nestor, E. N., & Giuseppe, C. (2006). Design and tests of a three finger hand with 1-DOF articulated fingers. *Robotica. 24(2)*, 183–196.

Ceccarelli, M., Rodriguez, N. E., & Carbone, G. (2006). Design and tests of a three finger hand with 1-DOF articulated fingers. *Robotica 24, no. 2*, 183-196.

Cipriani, C., Controzzi, M., & Carrozza, M. C. (2010). Objectives, criteria and methods for the design of the SmartHand transradial prosthesis. *Robotica 28, no. 6*, 919-927.

Crooks, W., Rozen-Levy, S., Trimmer, B., Rogers, C., & Messner, W. (2017). Passive gripper inspired by Manduca sexta and the Fin Ray® Effect. *International Journal of Advanced Robotic Systems 14.4*(14.4), 1729881417721155.

Cutkosky, M. R. (1989). On grasp choice, grasp models, and the design of hands for manufacturing tasks. *IEEE Transactions on robotics and automation 5, no. 3*, 269-279.

De Visser, H., & Herder, J. L. (2000). Force-directed design of a voluntary closing hand prosthesis. *JRRD: Journal of Rehabilitation Research and Development, 37 (3)*.

Diftler, M. A., Ambrose, R. O., Tyree, K. S., Goza, S. M., & Huber, E. L. (2004). A mobile autonomous humanoid assistant. *4th IEEE/RAS International Conference on Humanoid Robots* (pp. 133-148). IEEE.

Dollar, A. M., & Howe, R. D. (2006). A robust compliant grasper via shape deposition manufacturing. *IEEE/ASME transactions on mechatronics 11.2*, (pp. 154-131).

Doria, M., & Birglen, L. (2009). Design of an underactuated compliant gripper for surgery using nitinol. *Journal of Medical Devices 3, no. 1*.

Escriva, A. i. (2016). *Design of a Smart Gripper for Industrial Applications.* (Master's thesis).

Figliolini, G., & Ceccarelli, M. (2002). A novel articulated mechanism mimicking the motion of index fingers. *Robotica, 20(1)*, 13-22.

Gosselin, C. M., & Laliberte, T. (1998). *Underactuated Mechanical Finger with Return Actuation.* Washington, DC: U.S.: U.S. Patent No. US5,762,390.

Gosselin, C., Pelletier, F., & Laliberte, T. (2008). An anthropomorphic underactuated robotic hand with 15 dofs and a single actuator. *2008 IEEE International Conference on Robotics and Automation*, (pp. 749–754). Pasadena, CA, USA.

Guangbo, H., & Zhu, J. (2019). Design of a monolithic double-slider based compliant gripper with large displacement and anti-buckling ability. *Micromachines 10*, 665.

Hartenberg, R., & Denavit, J. (1964). *Kinematic synthesis of linkages.* New York: McGraw-Hill.

Hess-Coelho, T. A. (2007). A redundant parallel spherical linkage for robotic wrist application. *Journal of mechanical design*, 891-895.

Hirose, S., & Umetani, Y. (1978). The development of soft gripper for the versatile robot hand. *Mechanism and Machine Theory, vol 13(3)*, 351-359.

Kamikawa, Y., & Maeno, T. (2008). Underactuated five-finger prosthetic hand inspired by grasping force distribution of humans. *2008 IEEE/RSJ International Conference on Intelligent Robots and Systems*, (pp. 717–722).

Kaneko, M., & Tanie, K. (1994). Contact point detection for grasping of an unknown object using self-posture changeability. *IEEE Transactions on Robotics and Automation, 10(3)*, (pp. 355-367).

Khakpour, H., & Birglen, L. (2013). Numerical analysis of the grasp configuration of a planar 3-DOF linkage-driven underactuated finger. *Journal of Computational and Nonlinear Dynamics, 8(2).*

Kocabas, H. (2009). Gripper design with spherical parallelogram linkage. *Journal of mechanical design*.

Kok, Y. Y., & Low, K. H. (2018). Design and Evaluation of an Underactuated Adaptive Finger for Parallel Grippers. *2018 15th International Conference on Control, Automation, Robotics and Vision (ICARCV).* IEEE.

Kota, S., Lu, K.-J., Kreiner, Z., Trease, B., Arenas, J., & Geiger, J. (2005). Design and application of compliant mechanisms for surgical tools. 981-989.

Kragten, G. A., & Herder, J. L. (2010). The ability of underactuated hands to grasp and hold objects. *Mechanism and Machine Theory, 45(3)*, 408–425.

Krut, S. (2005). A force-isotropic underactuated finger. *Proceedings of the 2005 IEEE International Conference on Robotics and Automation*, (pp. 2314–2319).

Laliberté, T., & Gosselin, C. M. (1998). Simulation and design of underactuated mechanical hands. *Mechanism and Machine Theory, 33(1-2)*, 39–57.

Li, G., Zhang, C., Zhang, W., Sun, Z., & Chen, Q. (2014). Coupled and self-adaptive under-actuated finger with a novel s-coupled and secondly self-adaptive mechanism. *Journal of Mechanisms and Robotics 6.4*, 041010.

Lotti, F., & Vassura, G. (2002). A novel approach to mechanical design of articulated fingers for robotic hands. *IEEE/RSJ International Conference on Intelligent Robots and Systems* (pp. 1687-1692). IEEE.

McCarthy, J. M., & Soh, G. S. (2010). *Geometric Design of Linkages, 2nd Edition.* Springer.

McDonald, M., & Agrawal, S. K. (2010). Design of a bio-inspired spherical four-bar mechanism for flapping-wing micro air-vehicle applications. *Journal of Mechanical Robotics*, 021012.

Myszka, D. (2012). *Machines and Mechanisms: Applied Kinematic Analysis.* New Jersey: Pearson Education.

Nakanishi, H., & Yoshida, K. (2002). The tako (target collaborativize) flyer: a new concept for future satellite servicing. In *Smaller Satellites: Bigger Business?* (pp. 397-399). Dordrecht: Springer.

Norton, R. L. (2003). *Design of Machinery* . McGraw Hill.

Ozawa, R., Hashirii, K., & Kobayashi, H. (2009). Design and control of underactuated tendon-driven mechanisms. *2009 IEEE International Conference on Robotics and Automation*, (pp. 1522-1527).

Reddy, P. V., & Suresh, V. V. (2013). A review on importance of universal gripper in industrial robot applications. *Int. J. Mech. Eng. Robot. Res, 2(2), 2.2*(255-264), 255-264.

Shan, X., & Birglen, L. (2020). Modeling and analysis of soft robotic fingers using the fin ray effect. *The International Journal of Robotics Research 39.14*(39.14), 1686-1705.

Sie, L. M., & Gosselin, C. M. (2002). Dynamic simulation and optimization of underactuated robotic fingers. *International Design Engineering Technical Conferences and Computers and Information in Engineering Conference* (pp. 191–199). American Society of Mechanical Engineers.

Song, C., Chen, Y., & Chen, I.-M. (2013). A 6R linkage reconfigurable between the line-symmetric Bricard linkage and the Bennett linkage. *Mechanism and Machine Theory*, 278-292.

Song, X., Deng, Z., Guo, H., Liu, R., Li, L., & Liu, R. (2017). Networking of Bennett linkages and its application on deployable parabolic cylindrical antenna. *Mechanism and Machine Theory, Vol. 109*, 95-125.

Toussaint, G. (2003, June–July). Simple proofs of a geometric property of four-bar linkages. *The American Mathematical Monthly 110*, pp. 482-494.

Tubiana, R., Thomine, J.-M., & Mackin, E. (1998). *Examination of the hand and wrist.* CRC Press.

Wu, C., Liu, X.-J., Wang, L., & Wang, J. (2010). Optimal design of spherical 5R parallel manipulators considering the motion/force transmissibility. *Journal of mechanical design*.

Yu, Y., Luo, Y., & Li, L. (2007). Deployable membrane structure based on the Bennett linkage. *Proceedings of the Institution of Mechanical Engineers, Part G: Journal of Aerospace Engineering*, (pp. 775-783).

Zheng, E., & Zhang, W. (2019). An underactuated PASA finger capable of perfectly linear motion with compensatory displacement. *Journal of Mechanisms and Robotics 11.1*(11.1), 014505.

APPENDIX A JACOBIAN MATRICES

In this appendix, the different Jacobian matrices for all the fingers for all the contact scenarios are calculated. For the first mechanism, the equation

$$\boldsymbol{\delta}\mathbf{y}_j^i = \boldsymbol{\delta}\mathbf{r}_{P_j^i}^T \mathbf{y}_j^i \tag{6.1}$$

Is used in order to find an equation that relates $\boldsymbol{\delta}\mathbf{y}_1^1$ and $\boldsymbol{\delta}\mathbf{y}_2^1$ to δx_a^1 and $\delta\theta_{1,F}^1$, and δx_a^1 and $\delta\theta_{2,F}^1$ respectively.

$r_{P_j^i}$ is the vector from point $O_{j,F}^i$ to the contact point P_j^i which is at a distance k_j^i from the base of the corresponding phalanx, so for mechanism 1 and contact scenario 1, one can write:

$$\boldsymbol{r}_{P_1^1} = \begin{bmatrix} k_1^1 c_1^1 + x_a^1 \\ k_1^1 s_1^1 \end{bmatrix} \tag{6.2}$$

c_j^i and s_j^i have the same definitions as mentioned before in the kinetostatic analysis section of the article. After deriving this vector, one obtains:

$$\boldsymbol{\delta r}_{P_1^1} = \begin{bmatrix} -k_1^1 c_1^1 \delta\theta_{1,F}^1 - \delta x_a^1 \\ k_1^1 s_1^1 \delta\theta_{1,F}^1 \end{bmatrix} \tag{6.3}$$

One last vector is required before the calculation of $\boldsymbol{\delta}\mathbf{y}_1^1$, and that vector is $\mathbf{y}_1^1$, which defines the direction of the contact force generated by the finger in contact scenario 1 on the proximal phalanx:

$$\mathbf{y}_1^1 = \begin{bmatrix} -s_1^1 \\ c_1^1 \end{bmatrix} \tag{6.4}$$

$\boldsymbol{\delta}\mathbf{y}_1^1$ is then calculated:

$$\begin{aligned} \boldsymbol{\delta}\mathbf{y}_1^1 &= \boldsymbol{\delta r}_{P_1^1}.\mathbf{y}_1^1 \\ &= \begin{bmatrix} -k_1^1 c_1^1 \delta\theta_{1,F}^1 - \delta x_a^1 \\ k_1^1 s_1^1 \delta\theta_{1,F}^1 \end{bmatrix}.\begin{bmatrix} -s_1^1 \\ c_1^1 \end{bmatrix} \\ &= -s_1^1\left(-k_1^1 c_1^1 \delta\theta_{1,F}^1 - \delta x_a^1\right) + c_1^1(k_1^1 s_1^1 \delta\theta_{1,F}^1) \\ &= k_1^1 \delta\theta_{1,F}^1 - s_1^1 \delta x_a^1 \end{aligned} \tag{6.5}$$

Now using equ. (1) one finally obtains the Jacobian matrix $\mathbf{J}_1^1$ for mechanism 1 for contact scenario 1:

$$\begin{bmatrix} \delta x_a^1 \\ \delta y_1^1 \end{bmatrix} = \mathbf{J}_1^1 \begin{bmatrix} \delta x_a^1 \\ \delta\theta_{1,F}^1 \end{bmatrix} \tag{6.6}$$

With

$$\mathbf{J}_1^1 = \begin{bmatrix} 1 & 0 \\ -s_1^1 & k_1^1 \end{bmatrix} \tag{6.7}$$

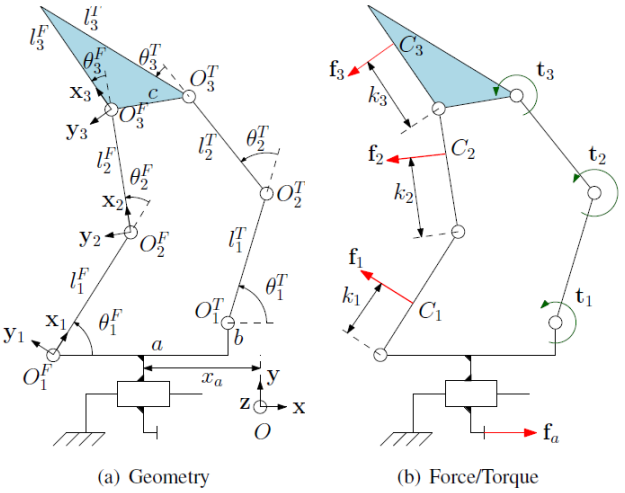

Figure 6.1 Parameters of the self-adaptive finger based on a six-bar, taken from (Birglen, 2019).

It should be noted that the exact same method can be applied to find the Jacobian matrix for the rest of the mechanisms for contact scenario 1 (contact on the proximal phalanx), so one obtains:

$$\mathbf{J}_1^2 = \begin{bmatrix} 1 & 0 \\ -s_1^2 & k_1^1 \end{bmatrix} \qquad \mathbf{J}_1^3 = \begin{bmatrix} 1 & 0 \\ -s_1^3 & k_1^1 \end{bmatrix}$$
$$\mathbf{J}_1^4 = \begin{bmatrix} 1 & 0 \\ -s_1^4 & k_1^1 \end{bmatrix} \tag{6.8}$$

The same procedure can be repeated to find $\mathbf{J}_2^i$ and $\mathbf{J}_3^i$ the Jacobian matrix for mechanism i for contact scenarios 2 and 3, but the calculations become more complex for the intermediate and distal phalanges, so another method will be used to calculate the remaining Jacobian matrices. This method is based on the Jacobian matrix calculated in [8] for the finger based on a 6-bar mechanism. Since this finger has three phalanges and 3 DOF, its Jacobian matrix is a 4×4 matrix and can be used to calculate the smaller matrices in the context of this paper. The Jacobian matrix calculated in [8] is defined as:

$$\boldsymbol{\delta X} = \mathbf{J}\,\boldsymbol{\delta\theta} \tag{6.9}$$

With

$$\mathbf{J} = \begin{bmatrix} 1 & 0 & 0 & 0 \\ -s_1 & k_1 & 0 & 0 \\ -s_{12} & l_1c_2 + k_2 & k_2 & 0 \\ -s_{123} & l_1c_{23} + l_2c_3 + k_3 & l_2c_3 + k_3 & k_3 \end{bmatrix}, \boldsymbol{\delta X} = \begin{bmatrix} \delta x_a \\ \delta y_1 \\ \delta y_2 \\ \delta y_3 \end{bmatrix}, \text{and } \boldsymbol{\delta\theta} = \begin{bmatrix} \delta x_a \\ \delta\theta_1^F \\ \delta\theta_2^F \\ \delta\theta_3^F \end{bmatrix} \tag{6.10}$$

All the parameters used in the expression of $\mathbf{J}$ can be identified in Figure 6.1. Now the Jacobian matrix for all the mechanisms for contact scenario 2, meaning for the contact with the distal

phalanx for mechanisms 1 and 2, and contact with the intermediate phalanx for mechanisms 3 and 4 can be calculated by calculating the expression of δy_2 in terms of the parameters on the right side of the equ. (6.11):

$$\delta y_2 = -s_{12}\,\delta x_a + (l_1 c_2 + k_2)\delta\theta_1^F + k_2\delta\theta_2^F \tag{6.11}$$

Now by replacing the parameters used in [8] by the ones used in this paper:

$$\delta y_2^i = -s_{12}^i\,\delta x_a^i + \left(l_{1,F}^i c_2^i + k_2^i\right)\delta\theta_{1,F}^i + k_2^i\delta\theta_{2,F}^i \tag{6.12}$$

Since all the mechanisms here have two DOF if the actuation of the base is considered, one should eliminate the third variable from the right side of equ. (6.13):

$$\delta y_2^i = -s_{12}^i\,\delta x_a^i + \left[\left(l_{1,F}^i c_2^i + k_2^i\right)\frac{\delta\theta_{1,F}^i}{\delta\theta_{2,F}^i} + k_2^i\right]\delta\theta_{2,F}^i \tag{6.13}$$

Let $X^i = \frac{\delta\theta_{1,F}^i}{\delta\theta_{2,F}^i}$ be the ratio between the angular velocity of the first and second joint in the linkage of the phalanges of the fingers. Finally, the Jacobian matrix for contact scenario 2 for all the mechanisms can be calculated:

$$\begin{bmatrix}\delta x_a^i \\ \delta y_2^i\end{bmatrix} = \mathbf{J}_2^i \begin{bmatrix}\delta x_a^i \\ \delta\theta_{2,F}^i\end{bmatrix}$$

With

$$\mathbf{J}_2^i = \begin{bmatrix} 1 & 0 \\ -s_{12}^i & \left(l_{1,F}^i c_2^i + k_2^i\right)X^i + k_2^i \end{bmatrix} \tag{6.14}$$

For $i = 1,2,3,4$

The Jacobian matrix for contact scenario 3 for mechanisms 3 and 4 can be calculated using the same method and it starts with calculating δy_3 in terms of the parameters in right hand side of equ. (6.15):

$$\delta y_3 = -s_{123}\delta x_a + (l_1 c_{23} + l_2 c_3 + k_3)\delta\theta_1^F + (l_2 c_3 + k_3)\delta\theta_2^F + k_3\delta\theta_3^F \tag{6.15}$$

Now replacing with the right parameters:

$$\delta y_3^i = -s_{123}^i\,\delta x_a^i + \left(l_{1,F}^i c_{23}^i + l_{2,F}^i c_3^i + k_3^i\right)\delta\theta_{1,F}^i + \left(l_{2,F}^i c_3^i + k_3^i\right)\delta\theta_{2,F}^i + k_3^i\delta\theta_{3,F}^i \tag{6.16}$$

By eliminating the two redundant variables one obtains:

$$\delta y_3^i = -s_{123}^i\,\delta x_a^i + \left[\left(l_{1,F}^i c_{23}^i + l_{2,F}^i c_3^i + k_3^i\right)\frac{\delta\theta_{1,F}^i}{\delta\theta_{3,F}^i} + \left(l_{2,F}^i c_3^i + k_3^i\right)\frac{\delta\theta_{2,F}^i}{\delta\theta_{3,F}^i} + k_3^i\right]\delta\theta_{3,F}^i \tag{6.17}$$

Let $Y^i = \frac{\delta\theta_{1,F}^i}{\delta\theta_{3,F}^i}$ and $Z^i = \frac{\delta\theta_{2,F}^i}{\delta\theta_{3,F}^i}$ be the ratios between the first and third joints and the second and third ones in the phalanges linkages of mechanisms 3 and 4 respectively. The Jacobian matrix for contact scenario 3 for fingers 3 and 4 can then be calculated:

$$\begin{bmatrix} \delta x_a^i \\ \delta y_3^i \end{bmatrix} = \mathbf{J}_3^i \begin{bmatrix} \delta x_a^i \\ \delta \theta_{3,F}^i \end{bmatrix}$$

With

$$\mathbf{J}_3^i = \begin{bmatrix} 1 & 0 \\ -s_{123}^i & \left(l_{1,F}^i c_{23}^i + l_{2,F}^i c_3^i + k_3^i\right) Y^i + \left(l_{2,F}^i c_3^i + k_3^i\right) Z^i + k_3^i \end{bmatrix} \tag{6.18}$$

For $i = 3,4$

APPENDIX B VELOCITY EQUATIONS

Velocity equations for mechanism 1:

The loop equations for mechanism 1 can be written as:

$$\begin{aligned} l_1^1\cos\left(\theta_{1,F}^1\right)+c^1\cos\left(\theta_{1,F}^1+\theta_{2,F}^1-\psi^1\right)&=a^1+b^1\cos\left(\theta_{1,T}^1\right)\\ l_1^1\sin\left(\theta_{1,F}^1\right)+c^1\sin\left(\theta_{1,F}^1+\theta_{2,F}^1-\psi^1\right)&=b^1\sin\left(\theta_{1,T}^1\right)\end{aligned} \tag{6.19}$$

By taking one element and isolating it in the left hand part of each equation one obtains the three sets of equations:

$$\begin{cases} b^1\cos\left(\theta_{1,T}^1\right)=l_1^1\cos\left(\theta_{1,F}^1\right)+c^1\cos\left(\theta_{1,F}^1+\theta_{2,F}^1-\psi^1\right)-a^1\\ \quad b^1\sin\left(\theta_{1,T}^1\right)=l_1^1\sin\left(\theta_{1,F}^1\right)+c^1\sin\left(\theta_{1,F}^1+\theta_{2,F}^1-\psi^1\right)\end{cases}$$

$$\begin{cases} l_1^1\cos\left(\theta_{1,F}^1\right)=a^1+b^1\cos\left(\theta_{1,T}^1\right)-c^1\cos\left(\theta_{1,F}^1+\theta_{2,F}^1-\psi^1\right)\\ \quad l_1^1\sin\left(\theta_{1,F}^1\right)=b^1\sin\left(\theta_{1,T}^1\right)-c^1\sin\left(\theta_{1,F}^1+\theta_{2,F}^1-\psi^1\right)\end{cases} \tag{6.20}$$

$$\begin{cases} c^1\cos\left(\theta_{1,F}^1+\theta_{2,F}^1-\psi^1\right)=a^1+b^1\cos\left(\theta_{1,T}^1\right)-l_1^1\cos\left(\theta_{1,F}^1\right)\\ \quad c^1\sin\left(\theta_{1,F}^1+\theta_{2,F}^1-\psi^1\right)=b^1\sin\left(\theta_{1,T}^1\right)-l_1^1\sin\left(\theta_{1,F}^1\right)\end{cases}$$

Now from each set of equations we can calculate a single one by squaring and adding the two equations in this set:

For the first set:

$$\begin{aligned} {b^1}^2=&\left(l_1^1\cos\left(\theta_{1,F}^1\right)+c^1\cos\left(\theta_{1,F}^1+\theta_{2,F}^1-\psi^1\right)-a^1\right)^2+\\ &\left(l_1^1\sin\left(\theta_{1,F}^1\right)+c^1\sin\left(\theta_{1,F}^1+\theta_{2,F}^1-\psi^1\right)\right)^2\end{aligned} \tag{6.21}$$

$$\begin{aligned} {b^1}^2=&{l_1^1}^2+{c^1}^2+{a^1}^2+2l_1^1c^1\left(\cos\left(\theta_{1,F}^1\right)\cos\left(\theta_{1,F}^1+\theta_{2,F}^1-\psi^1\right)+\right.\\ &\left.\sin\left(\theta_{1,F}^1\right)\sin\left(\theta_{1,F}^1+\theta_{2,F}^1-\psi^1\right)\right)-2a^1c^1\cos\left(\theta_{1,F}^1+\theta_{2,F}^1-\psi^1\right)-\\ &2l_1^1a^1\cos\left(\theta_{1,F}^1\right)\end{aligned} \tag{6.22}$$

For the second set:

$$\begin{aligned} {l_1^1}^2=&\\ &\left(a^1+b^1\cos\left(\theta_{1,T}^1\right)-c^1\cos\left(\theta_{1,F}^1+\theta_{2,F}^1-\psi^1\right)\right)^2+\left(b^1\sin\left(\theta_{1,T}^1\right)-\\ &c^1\sin\left(\theta_{1,F}^1+\theta_{2,F}^1-\psi^1\right)\right)^2\end{aligned} \tag{6.23}$$

$$
\begin{aligned}
{l_1^1}^2 = {a^1}^2 + {b^1}^2 + {c^1}^2 + 2a^1b^1\cos\left(\theta_{1,T}^1\right) \\
- 2a^1c^1\cos\left(\theta_{1,F}^1 + \theta_{2,F}^1 - \psi^1\right) \\
- 2b^1c^1\left(\cos\left(\theta_{1,T}^1\right)\cos\left(\theta_{1,F}^1 + \theta_{2,F}^1 - \psi^1\right)\right. \\
\left. + \sin\left(\theta_{1,T}^1\right)\sin\left(\theta_{1,F}^1 + \theta_{2,F}^1 - \psi^1\right)\right)
\end{aligned}
\tag{6.24}
$$

For the third one:

$$
{c^1}^2 = \left(a^1 + b^1\cos\left(\theta_{1,T}^1\right) - l_1^1\cos\left(\theta_{1,F}^1\right)\right)^2 + \left(b^1\sin\left(\theta_{1,T}^1\right) - l_1^1\sin\left(\theta_{1,F}^1\right)\right)^2
$$

$$
\begin{aligned}
{c^1}^2 = {a^1}^2 + {b^1}^2\cos^2\left(\theta_{1,T}^1\right) + {l_1^1}^2\cos^2\left(\theta_{1,F}^1\right) \\
+ 2\left(b^1a^1\cos\left(\theta_{1,T}^1\right) - b^1l_1^1\cos\left(\theta_{1,T}^1\right)\cos\left(\theta_{1,F}^1\right)\right. \\
\left. - l_1^1a^1\cos\left(\theta_{1,F}^1\right)\right) + {b^1}^2\sin^2\left(\theta_{1,T}^1\right) - {l_1^1}^2\sin^2\left(\theta_{1,F}^1\right) \\
- 2b^1l_1^1\sin\left(\theta_{1,T}^1\right)\sin\left(\theta_{1,F}^1\right)
\end{aligned}
\tag{6.25}
$$

$$
{c^1}^2 = {a^1}^2 + {b^1}^2 + {l_1^1}^2 + 2\left(a^1b^1\cos\left(\theta_{1,T}^1\right) + l_1^1a^1\cos\left(\theta_{1,F}^1\right) + b^1l_1^1\cos\left(\theta_{1,T}^1 - \theta_{1,F}^1\right)\right)
$$

Now by deriving the obtained equations we can obtain the velocity equations of mechanism 1:

$$
\frac{\dot{\theta_{1,T}^1}}{\dot{\theta_{1,F}^1}} = \frac{\delta\theta_{1,T}^1}{\delta\theta_{1,F}^1} = \frac{l_1^1\left(b^1\sin\left(\theta_{1,T}^1 - \theta_{1,F}^1\right) - a^1\sin\left(\theta_{1,F}^1\right)\right)}{b^1\left(l_1^1\sin\left(\theta_{1,T}^1 - \theta_{1,F}^1\right) - a^1\sin\left(\theta_{1,T}^1\right)\right)}
$$

$$
\frac{\dot{\theta_{1,F}^1}}{\dot{\theta_{2,F}^1}} = \frac{\delta\theta_{1,T}^1}{\delta\theta_{1,F}^1} = \frac{-\left(l_1^1c^1\sin\left(\psi^1 - \theta_{2,F}^1\right) - c^1a^1\sin\left(\theta_{1,F}^1 + \theta_{2,F}^1 - \psi^1\right)\right)}{\left(l_1^1a^1\sin\left(\theta_{1,F}^1\right) - a^1c^1\sin\left(\theta_{1,F}^1 + \theta_{2,F}^1 - \psi^1\right)\right)}
\tag{6.26}
$$

$$
\begin{aligned}
\dot{\theta_{1,T}^1}\left(2b^1c^1\sin\left(\theta_{1,T}^1 + \psi^1 - \theta_{2,F}^1 - \theta_{1,F}^1\right) - 2\,a^1b^1\sin\left(\theta_{1,T}^1\right)\right) + \\
\dot{\theta_{2,F}^1}\left(2a^1c^1\sin\left(\theta_{1,F}^1 + \theta_{2,F}^1 - \psi^1\right) - 2b^1c^1\sin\left(\theta_{1,T}^1 + \psi^1 - \theta_{2,F}^1 - \theta_{1,F}^1\right)\right) + \dot{\theta_{1,F}^1}\left(2a^1c^1\sin\left(\theta_{1,F}^1 + \theta_{2,F}^1 - \psi^1\right) - 2b^1c^1\sin\left(\theta_{1,T}^1 + \psi^1 - \theta_{2,F}^1 - \theta_{1,F}^1\right)\right) = 0
\end{aligned}
$$

The last equation should be divided by $\dot{\theta_{1,F}^1}$ in order to find $\frac{\dot{\theta_{2,F}^1}}{\dot{\theta_{1,F}^1}}$. All the other velocity equations of this finger can be found by combining the three equations calculated.

Velocity equations for mechanisms 2:

The loop equations for mechanism 2 can be written as:

$$\begin{aligned} l_1^2\cos\left(\theta_{1,F}^2\right)+b^2\cos\left(\theta_{1,F}^2+\theta_{2,F}^2-\psi^2\right)&=a^2+x_T^2\cos(\theta_T^2)\\ l_1^1\sin\left(\theta_{1,F}^2\right)+b^2\sin\left(\theta_{1,F}^2+\theta_{2,F}^2-\psi^2\right)&=x_T^2\sin(\theta_T^2)\end{aligned} \tag{6.27}$$

By taking one element and isolating it in the left hand part of each equation one obtains the sets of equations:

$$\begin{cases} b^2\cos\left(\theta_{1,F}^2+\theta_{2,F}^2-\psi^2\right)=a^2+x_T^2\cos(\theta_T^2)-l_1^2\cos\left(\theta_{1,F}^2\right)\\ \quad b^2\sin\left(\theta_{1,F}^2+\theta_{2,F}^2-\psi^2\right)=x_T^2\sin(\theta_T^2)-l_1^1\sin\left(\theta_{1,F}^2\right)\end{cases}$$
$$\begin{cases} l_1^2\cos\left(\theta_{1,F}^2\right)=a^2+x_T^2\cos(\theta_T^2)-b^2\cos\left(\theta_{1,F}^2+\theta_{2,F}^2-\psi^2\right)\\ \quad l_1^1\sin\left(\theta_{1,F}^2\right)=x_T^2\sin(\theta_T^2)-b^2\sin\left(\theta_{1,F}^2+\theta_{2,F}^2-\psi^2\right)\end{cases} \tag{6.28}$$

And instead of taking a third set of equations, it was decided to consider a new equation based on the geometry of the mechanism:

$$\mathbf{u}_{b^2}.\mathbf{u}^T=\|\mathbf{u}_{b^2}\|\|\mathbf{u}^T\|\cos(\alpha) \tag{6.29}$$

With $\mathbf{u}_{b^2}$ being the unitary vector having the same direction as the link $O_{2,F}^2O_{2,T}^2$ and $\mathbf{u}^T$ the unitary vector that has the same direction as the link $O_{1,T}^2O_{2,T}^2$.

Now the same procedure is applied to the two sets of equations: squaring and adding in order to end up with two equations to use along with the third one in order to get the three velocity equations that will be used to calculate all the other equations:

For the first set:

$$\begin{aligned} {b^2}^2&=\left(a^2+x_T^2\cos(\theta_T^2)-l_1^2\cos\left(\theta_{1,F}^2\right)\right)^2+\left(x_T^2\sin(\theta_T^2)-l_1^1\sin\left(\theta_{1,F}^2\right)\right)^2\\ {b^2}^2&={a^2}^2+{x_T^2}^2+{l_1^2}^2+2\left(a^2x_T^2\cos(\theta_T^2)-a^2l_1^2\cos\left(\theta_{1,F}^2\right)-\right.\\ &\left.l_1^2x_T^2\cos\left(\theta_T^2-\theta_{1,F}^2\right)\right)\end{aligned} \tag{6.30}$$

For the second set:

$$\begin{aligned} {l_1^2}^2&=\left(a^2+x_T^2\cos(\theta_T^2)-b^2\cos\left(\theta_{1,F}^2+\theta_{2,F}^2-\psi^2\right)\right)^2+\left(x_T^2\sin(\theta_T^2)-\right.\\ &\left.b^2\sin\left(\theta_{1,F}^2+\theta_{2,F}^2-\psi^2\right)\right)^2\end{aligned} \tag{6.31}$$

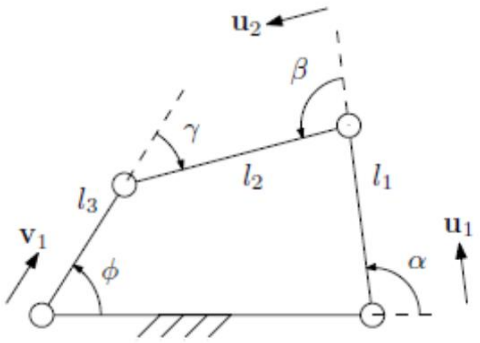

Figure 6.2 Parameters of a general four-bar mechanism,
taken from (Birglen, 2019)

Finally, by deriving those two equations, one will be able to combine them with the third one based on the geometry on the mechanism to calculate the velocity equations $\frac{\dot{\theta}_{1,F}^2}{\dot{\theta}_T^2}$, $\frac{\dot{\theta}_{1,F}^2}{\dot{\theta}_{2,F}^2}$, and $\frac{\dot{x}_T^2}{\dot{\theta}_{2,F}^2}$, and with those, one can combine them to find the remaining ones.

Velocity equations for mechanism 3:

Although the velocity equation of mechanism 3 can be calculating using the same method used to calculate those of mechanism 1, a different approach was considered here for the sake of simplicity.

Let us assume the general model of a 4-bar linkage as illustrated in Figure 6.2. Considering the geometrical loop closure equation and taking the derivative of it with respect to time:

$$\dot{\alpha} l_1 \mathbf{E}\mathbf{u_1} = \dot{\emptyset}(l_3 \mathbf{E}\mathbf{v_1} - l_2 \mathbf{E}\mathbf{u_2}) - \dot{\boldsymbol{\gamma}} \mathbf{E}\mathbf{u_2} \tag{6.32}$$

Where

$$\mathbf{E} = \begin{bmatrix} 0 & -1 \\ 1 & 0 \end{bmatrix}$$

Is the matrix allowing to compute vector cross products in the plane and $\mathbf{u_1}$, $\mathbf{u_2}$, and $\mathbf{v_1}$ are the unit vectors along the different links of the 4-bar as seen in Figure 6.2 Parameters of a general four-bar mechanism.

If $\emptyset$ is considered to be the input angle, and all the other angles are considered as outputs, one can write:

$$\begin{bmatrix}\dot{\alpha}\\ \dot{\beta}\\ \dot{\gamma}\end{bmatrix} = A^{-1}V\dot{\emptyset} \tag{6.33}$$

Where

$$V = \begin{bmatrix} l_3\mathbf{Ev_1} - \frac{l_2}{2}\mathbf{Eu_2} \\ 1 \end{bmatrix} \qquad \mathbf{A} = \begin{bmatrix} l_1\mathbf{Eu_1} & 0 & l_2\mathbf{Eu_2} \\ 1 & 1 & -1 \end{bmatrix} \tag{6.34}$$

The equation then becomes:

$$\begin{bmatrix} l_1\mathbf{Eu_1} & 0 & l_2\mathbf{Eu_2} \\ 1 & 1 & -1 \end{bmatrix}_{3\times3} \begin{bmatrix}\dot{\alpha}\\ \dot{\beta}\\ \dot{\gamma}\end{bmatrix} = \begin{bmatrix} l_3\mathbf{Ev_1} - \frac{l_2}{2}\mathbf{Eu_2} \\ 1 \end{bmatrix}_{3\times1} \dot{\emptyset} \tag{6.35}$$

The unitary vectors are then calculated:

$$\mathbf{u}_1 = \begin{bmatrix} \cos(\theta_T^3 + \frac{\pi}{2}) \\ \sin(\theta_T^3 + \frac{\pi}{2}) \end{bmatrix} \qquad \mathbf{u}_2 = \begin{bmatrix} -\cos(\theta_{1,F}^3 + \theta_{2,F}^3) \\ -\sin(\theta_{1,F}^3 + \theta_{2,F}^3) \end{bmatrix} \tag{6.36}$$

$$\mathbf{v}_1 = \begin{bmatrix} \cos(\theta_{1,F}^3) \\ \sin(\theta_{1,F}^3) \end{bmatrix}$$

Now for the calculation of Matrix A:

$$\begin{bmatrix} A_{11} \\ A_{21} \end{bmatrix} = l_1\mathbf{Eu_1}$$

$$= l_1 \begin{bmatrix} 0 & -1 \\ 1 & 0 \end{bmatrix} \begin{bmatrix} \cos(\theta_T^3 + \frac{\pi}{2}) \\ \sin(\theta_T^3 + \frac{\pi}{2}) \end{bmatrix} \tag{6.37}$$

$$= l_1 \begin{bmatrix} -\sin(\theta_T^3 + \frac{\pi}{2}) \\ \cos(\theta_T^3 + \frac{\pi}{2}) \end{bmatrix}$$

$$= \begin{bmatrix} -l_1 \sin\left(\theta_T^3 + \frac{\pi}{2}\right) \\ l_1 \cos(\theta_T^3 + \frac{\pi}{2}) \end{bmatrix}$$

$$\begin{bmatrix} A_{12} \\ A_{22} \end{bmatrix} = l_2 \mathbf{Eu_2}$$

$$= l_2 \begin{bmatrix} 0 & -1 \\ 1 & 0 \end{bmatrix} \begin{bmatrix} -\cos(\theta_{1,F}^3 + \theta_{2,F}^3) \\ -\sin(\theta_{1,F}^3 + \theta_{2,F}^3) \end{bmatrix} \quad (6.38)$$

$$= \begin{bmatrix} l_2 \sin(\theta_{1,F}^3 + \theta_{2,F}^3) \\ -l_2 \cos(\theta_{1,F}^3 + \theta_{2,F}^3) \end{bmatrix}$$

To finally obtain:

$$A = \begin{bmatrix} -l_1 \sin\left(\theta_T^3 + \frac{\pi}{2}\right) & 0 & l_2 \sin(\theta_{1,F}^3 + \theta_{2,F}^3) \\ l_1 \cos(\theta_T^3 + \frac{\pi}{2}) & 0 & -l_2 \cos(\theta_{1,F}^3 + \theta_{2,F}^3) \\ 1 & 1 & 1 \end{bmatrix} \quad (6.39)$$

And the calculation of the vector V:

$$\begin{bmatrix} V_1 \\ V_2 \end{bmatrix} = l_3 \mathbf{Ev_1} - \frac{l_2}{2} \mathbf{Eu_2}$$

$$= l_3 \begin{bmatrix} 0 & -1 \\ 1 & 0 \end{bmatrix} \begin{bmatrix} \cos(\theta_{1,F}^3) \\ \sin(\theta_{1,F}^3) \end{bmatrix} - \begin{bmatrix} \frac{l_2}{2} \sin(\theta_{1,F}^3 + \theta_{2,F}^3) \\ -\frac{l_2}{2} \cos(\theta_{1,F}^3 + \theta_{2,F}^3) \end{bmatrix}$$

$$= \begin{bmatrix} -l_3 \sin(\theta_{1,F}^3) \\ l_3 \cos(\theta_{1,F}^3) \end{bmatrix} - \begin{bmatrix} \frac{l_2}{2} \sin(\theta_{1,F}^3 + \theta_{2,F}^3) \\ -\frac{l_2}{2} \cos(\theta_{1,F}^3 + \theta_{2,F}^3) \end{bmatrix} \quad (6.40)$$

$$= \begin{bmatrix} -l_3 \sin\left(\theta_{1,F}^3\right) - \frac{l_2}{2} \sin(\theta_{1,F}^3 + \theta_{2,F}^3) \\ l_3 \cos\left(\theta_{1,F}^3\right) + \frac{l_2}{2} \cos(\theta_{1,F}^3 + \theta_{2,F}^3) \end{bmatrix}$$

To finally obtain:

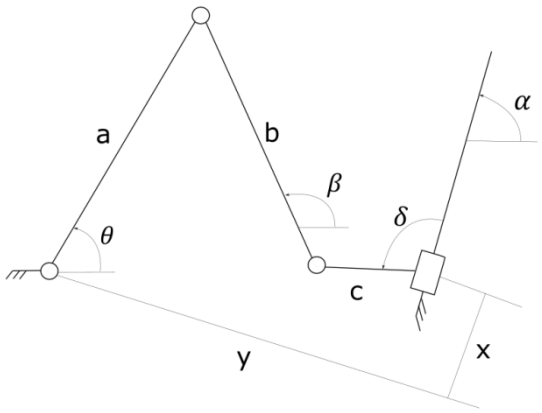

Figure 6.3 Parameters of a general slider-crank

$$V = \begin{bmatrix} -l_3 \sin\left(\theta_{1,F}^3\right) - \frac{l_2}{2}\sin(\theta_{1,F}^3 + \theta_{2,F}^3) \\ l_3 \cos\left(\theta_{1,F}^3\right) + \frac{l_2}{2}\cos(\theta_{1,F}^3 + \theta_{2,F}^3) \\ 1 \end{bmatrix} \tag{6.41}$$

The velocity equations of mechanism 3 can be calculated by setting $\dot{\phi} = \dot{\theta_{1,F}^3}$, $\dot{\alpha} = \dot{\theta_T^3}$, $\dot{\beta} = -\dot{\theta_{3,F}^3}$, and $\dot{\gamma} = \dot{\theta_{2,F}^3}$ and replacing the different parameters used by their appropriate equivalents. The three velocity equations are then calculated using:

$$\begin{bmatrix} \dot{\theta_{2,F}^3} \\ -\dot{\theta_{3,F}^3} \\ \dot{\theta_T^3} \end{bmatrix} = A^{-1} V \, \dot{\theta_{1,F}^3} \tag{6.42}$$

Velocity equations for mechanism 4:

This mechanism is a simple crank-slider and the general velocity equations can be applied to calculate the velocity equations of the crank-slider used in the context of this paper. For a general slider-crank, like the one shown in Figure x, one can compute the velocity equations:

$$\frac{\dot{x}}{\dot{\theta}} = \frac{a\sin(\beta - \theta)}{\cos(\alpha - \beta)}$$

$$\frac{\dot{\beta}}{\dot{\theta}} = \frac{a\cos(\theta)}{b\cos(\beta)} \tag{6.43}$$

$$\vec{x} + \vec{y} = \vec{a} + \vec{b} + \vec{c}$$

By replacing the appropriate parameters of the finger introduced in this work in these three equations, the calculation of the three velocity equations that can be used to calculate all the other ones needed will be possible.

APPENDIX C PARAMETERS OF THE MECHANISMS FUNCTION OF THE INPUT ANGLE

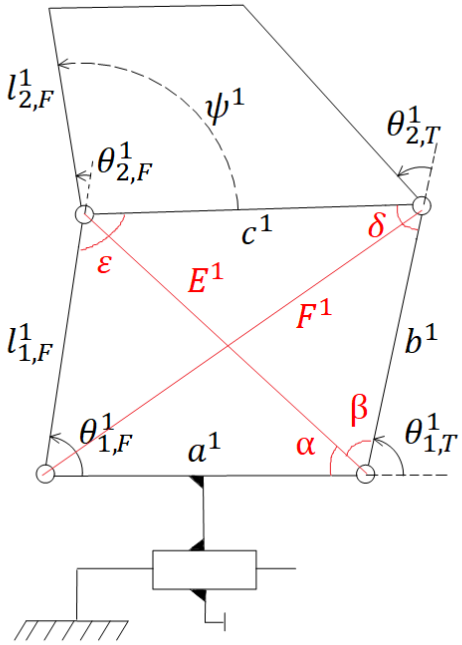

Figure 6.4 Parameters of finger #1

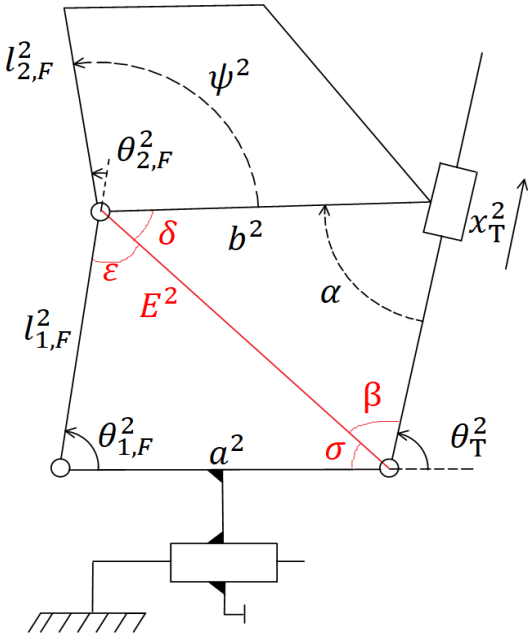

Figure 6.7 Parameters of finger #2

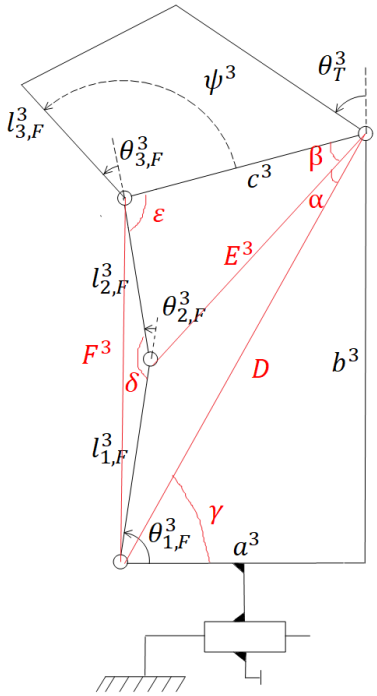

Figure 6.5 Parameters of finger #3

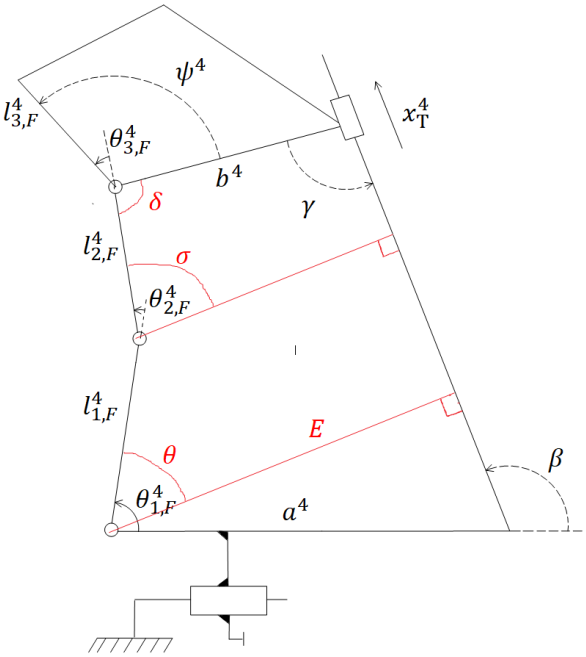

Figure 6.6 Parameters of finger #4

Angles calculation for mechanism 1:

To make the calculation of the different parameters of the mechanism easier, some additional parameters shown in Figure 6.4 have to be defined:

$$E^{1^2} = l_1^{1^2} + a^{1^2} - 2l_1^{1^2}a^{1^2}\cos(\theta_{1,F}^1)$$

And

$$F^{1^2} = l_1^{1^2} + c^{1^2} - 2l_1^{1^2}c^{1^2}\cos(\varepsilon)$$

E^1 and F^1 are used to calculate the angles $\alpha, \beta, \delta,$ and ε that will be used to calculate the parameters of the mechanism used in the article:

$$l_1^{1^2} = E^{1^2} + a^{1^2} - 2E^{1^2}a^{1^2}\cos(\alpha)$$

$$c^{1^2} = E^{1^2} + b^{1^2} - 2E^{1^2}b^{1^2}\cos(\beta)$$

$$\alpha = \cos^{-1}\left(\frac{E^{1^2} + a^{1^2} - l_1^{1^2}}{2E^{1^2}a^{1^2}}\right)$$

$$\beta = \cos^{-1}\left(\frac{E^{1^2} + b^{1^2} - c^{1^2}}{2E^{1^2}b^{1^2}}\right)$$

$$E^{1^2} = c^{1^2} + b^{1^2} - 2c^{1^2}b^{1^2}\cos(\delta)$$

$$\delta = \cos^{-1}\left(\frac{c^{1^2} + b^{1^2} - E^{1^2}}{2c^{1^2}b^{1^2}}\right)$$

$$F^{1^2} = b^{1^2} + a^{1^2} - 2b^{1^2}a^{1^2}\cos(\alpha + \beta)$$

$$\varepsilon = \cos^{-1}\left(\frac{l_1^{1^2} + c^{1^2} - F^{1^2}}{2l_1^{1^2}c^{1^2}}\right)$$

Finally the parameters $\theta_{2,F}^1, \theta_{1,T}^1, and\ \theta_{2,T}^1$ are calculated:

- $\pi = \varepsilon + \left(\psi^1 - \theta_{2,F}^1\right)$
  $\theta_{2,F}^1 = \varepsilon + \psi^1 - \pi$
- $\pi = \delta + k + \theta_{2,T}^1$
  $\theta_{2,T}^1 = \pi - \delta - k$
- $\pi = \alpha + \beta + \theta_{1,T}^1$
  $\theta_{1,T}^1 = \pi - (\alpha + \beta)$

Angles calculation for mechanism 2:

E^2 as seen in Figure 6.7 is defined as:

$$E^{2^2} = l_1^{2^2} + a^{2^2} - 2l_1^{2^2}a^{2^2}\cos(\theta_{1,F}^2)$$

It is used to calculate the angles $\sigma, \beta, \delta,$ and ε as seen in the figure:

$$\frac{E^2}{\sin\left(\theta_{1,F}^2\right)} = \frac{l_1^2}{\sin(\sigma)}$$

$$\sigma = \sin^{-1}\left(\frac{l_1^2\sin\left(\theta_{1,F}^2\right)}{E^2}\right)$$

$$\frac{b^2}{\sin(\beta)} = \frac{E^2}{\sin(\alpha)}$$

$$\beta = \sin^{-1}\left(\frac{b^2\sin(\alpha)}{E^2}\right)$$

$$\pi = \delta + \beta + \alpha$$

$$\delta = \pi - \beta - \alpha$$

$$\pi = \varepsilon + \beta + \sigma$$

$$\varepsilon = \pi - \beta - \sigma$$

Finally, the parameters $x_T^2, \theta_{2,F}^2$ and θ_T^2 are calculated:

$$\frac{x_T^2}{\sin(\delta)} = \frac{E^2}{\sin(\alpha)}$$

$$x_T^2 = \frac{E^2\sin(\delta)}{\sin(\alpha)}$$

$$\theta_{2,F}^2 = \varepsilon + \delta - \pi - \psi^2$$

$$\theta_T^2 = \pi - \sigma - \beta$$

Angles calculation for mechanism 3:

The parameters D and γ shown in Figure 6.5 are introduced to make the calculations easier:

$$D = \sqrt{{a^3}^2 + {b^3}^2}$$

$$\gamma = \tan^{-1}\left(\frac{b^3}{a^3}\right)$$

Now for the calculation of E^3 and F^3 that are used for the calculations of the angles later on:

$${E^3}^2 = {l_{1,F}^3}^2 + D^2 - 2{l_{1,F}^3}^2 D^2 \cos(\theta_{1,F}^3 - \gamma)$$

$${F^3}^2 = {c^3}^2 + D^2 - 2{c^3}^2 D^2 \cos(\alpha + \beta)$$

The angles $\alpha\ \beta\ \varepsilon\ \delta$ are calculated using the previous equations:

$$\alpha = \sin^{-1}\left(\frac{l_{1,F}^3 \sin(\theta_{1,F}^3 - \gamma)}{E^3}\right)$$

$$\beta = \cos^{-1}\left(\frac{{E^3}^2 + {c^3}^2 - {l_{2,F}^3}^2}{2E^3 c^3}\right)$$

$$\varepsilon = \cos^{-1}\left(\frac{{l_{2,F}^3}^2 + {c^3}^2 - {E^3}^2}{2l_{2,F}^3\, c^3}\right)$$

$$\delta = \cos^{-1}\left(\frac{{l_{2,F}^3}^2 + {l_{1,F}^3}^2 - {F^3}^2}{2l_{2,F}^3 l_{1,F}^3}\right)$$

Finally the parameters of the finger are calculated:

$$\theta_{2,F}^3 = \pi - \delta$$

$$\theta_{3,F}^3 = \varepsilon + \psi^3 - \pi$$

$$\theta_{\mathrm{T}}^3 = \frac{\pi}{2} + \gamma - \alpha - \beta - k$$

Angles calculation for mechanism 4:

The parameters $\theta, \sigma, \delta,$ and E seen in Figure 6.6 are introduced as:

$$\theta = \theta_{1,F}^4 - \left(\beta - \frac{\pi}{2}\right)$$

$$E = a^4 \cos\left(\beta - \frac{\pi}{2}\right)$$

$$\sigma = \cos^{-1}\left(\frac{E - l_{1,F}^4 \cos(\theta) - b^4 \cos\left(\frac{\pi}{2} - \gamma\right)}{l_{2,F}^4}\right)$$

$$\delta = 2\pi - \sigma - \gamma - \frac{\pi}{2}$$

And they are used to calculate the different parameters of the finger:

$$\theta_{2,F}^4 = \sigma - \theta$$

$$\theta_{3,F}^4 = \delta - \gamma + \psi^4 - \frac{\pi}{2}$$

As for x_T^4, it is divided into two parameters x_1 and x_2 as follows:

$$x_1 = l_{1,F}^4 \sin(\theta) + l_{2,F}^4 \sin(\sigma) + b^4 \sin\left(\frac{\pi}{2} - \gamma\right)$$

$$x_2 = a^4 \cos(\pi - \beta)$$

$$x_T^4 = x_1 + x_2$$